

COMPUTATIONAL FLUID DYNAMICS ANALYSIS OF STORE SEPARATION

A THESIS SUBMITTED TO
THE GRADUATE SCHOOL OF NATURAL AND APPLIED SCIENCES
OF
THE MIDDLE EAST TECHNICAL UNIVERSITY

BY

H. ÖZGÜR DEMİR

IN PARTIAL FULFILLMENT OF THE REQUIREMENTS
FOR
THE DEGREE OF MASTER OF SCIENCE
IN
AEROSPACE ENGINEERING

AUGUST 2004

Approval of the Graduate School of Natural and Applied Sciences.

Prof. Dr. Canan Özgen
Director

I certify that this thesis satisfies all the requirements as a thesis for the degree of Master of Science.

Prof. Dr. Nafiz Alemdaroğlu
Head of Department

This is to certify that we have read this thesis and that in our opinion it is fully adequate, in scope and quality, as a thesis for the degree of Master of Science.

Prof. Dr. Nafiz Alemdaroğlu
Supervisor

Examining Committee Members

Prof. Dr. Kahraman Albayrak

Prof. Dr. Nafiz Alemdaroğlu

Assoc. Prof. Dr. Sinan Eyi

Assoc. Prof. Dr. Serkan Özgen

Assoc. Prof. Dr. Yusuf Özyörük

I hereby declare that all information in this document has been obtained and presented in accordance with academic rules and ethical conduct. I also declare that, as required by these rules and conduct, I have fully cited and referenced all material and results that are not original to this work.

Name, Last name : H. Özgür Demir

Signature :

ABSTRACT

COMPUTATIONAL FLUID DYNAMICS ANALYSIS OF STORE SEPARATION

Demir, H. Özgür

M.S., Department of Aerospace Engineering

Supervisor: Prof. Dr. Nafiz Alemdaroğlu

August 2004, 83 pages

In this thesis, store separation from two different configurations are solved using computational methods. Two different commercially available CFD codes; *CFD-FASTAN*, an implicit Euler solver, and an unsteady panel method solver *USAERO*, coupled with integral boundary layer solution procedure are used for the present computations. The computational trajectory results are validated against the available experimental data of a generic wing-pylon-store configuration at Mach 0.95. Major trends of the separation are captured. Same configuration is used for the comparison of unsteady panel method with Euler solution at Mach 0.3 and 0.6. Major trends are similar to each other while some differences

in lateral and longitudinal displacements are observed. Trajectories of a fuel tank separated from an F-16 fighter aircraft wing and full aircraft configurations are found at Mach 0.3 using only the unsteady panel code. The results indicate that the effect of fuselage is to decrease the drag and to increase the side forces acting on the separating fuel tank from the aircraft. It is also observed that the yawing and rolling directions of the separating fuel tank are reversed when it is separated from the full aircraft configuration when compared to the separation from the wing alone configuration.

Keywords: CFD, Store Separation, Chimera, Overset Grids, CFD-FASTRAN, USAERO, Euler, Panel method

ÖZ

HARİCİ YÜK AYRILMASININ HESAPLAMALI AKIŞKANLAR DİNAMİĞİ İLE ANALİZİ

Demir, H. Özgür

Yüksek Lisans, Havacılık ve Uzay Mühendisliği Bölümü

Tez Yöneticisi: Prof. Dr. Nafiz Alemdaroğlu

Ağustos 2004, 83 sayfa

Bu çalışmada, iki farklı konfigürasyondan harici yük ayrılması problemi hesaplamalı akışkanlar yöntemleri kullanılarak çözülmüştür. Sonuçların elde edilmesinde iki farklı hesaplamalı akışkanlar dinamiği ticari yazılım paketi kullanılmıştır. Bunlar, CFD-FASTRAN Euler çözücüsü, ve zamana bağlı panel metodu ile birlikte entegral sınır tabaka yöntemini kullanan USAERO'dur. Jenerik kanat-pilon-harici yük konfigürasyonunun Mach 0.95 akış şartlarında hesaplanan yörünge sonuçları, rüzgar tüneli test sonuçları ile karşılaştırılmıştır. Ayrılma esnasındaki önemli değişimler, hesaplamalı akışkanlar dinamiği yöntemleri ile gözlenmiştir. Aynı konfigürasyon, Mach 0.3 ve 0.6 akış şartlarında zamana bağlı panel metodu

ve Euler çözümlerinin karşılaştırılmasında da kullanılmıştır. Yörünge üzerindeki temel değişimler birbirine benzer olup yanal ve boylamsal yöndeki yerdeğiştirme-lerde farklılıklar görülmüştür. F-16 savaş uçağının kanadına ve tüm uçağa ait konfigürasyonlardan Mach 0.3 akış şartlarında ayrılan bir yakıt tankının izlediği yörünge, zamana bağlı panel metodu ile bulunmuştur. Uçak gövdesinin yakıt tankının ayrılmasına olan etkisi, yakıt tankı üzerine etkiyen sürüklenme kuvvetinin azalması ve yanal kuvvetin artması yönündedir. Aynı ayrılma durumunda, yakıt tankının ayrılma sonrasındaki sapma ve yalpalama hareketlerinin yönlerinin de değiştiği gözlenmiştir.

Anahtar Kelimeler: HAD, Harici Yük Ayrılması, Chimera, Üst Üste Binen Ağ Sistemi, CFD-FASTRAN, USAERO, Euler, Panel metodu

to my family, for their endless support...

ACKNOWLEDGMENTS

I want to state my thanks to

Prof. Dr. Nafiz Alemdarođlu for his supervision, encouragement and patience during all stages of this thesis. His great ability to foresee the future needs of our country makes this thesis valuable for all whom interested in this subject.

Assoc. Prof. Dr. Yusuf Özyörük for his support, comments and suggestions, and *Prof. Dr. İsmail Hakkı Tuncer* for his technical support about the hardware and software needs during this thesis.

My friends from Aerospace Engineering Department, especially to *Mustafa Kaya* for his endless technical assistance and moral support in all of the stages of this thesis. His endless effort is highly appreciated. I would like to extend my thanks to *D. Funda Kurtuluş* for her support and help in the learning stages of the software, to *Y. Barbaros Ulusoy* for being a right hand for me when I needed help, to *Ömer Onur* and *Özhan Öksüz* for their useful suggestions and friendship.

Erhan Tarhan for his suggestions and precious contribution to this thesis. I would like to thank to *Keith Jordan* from CFDRC for his invaluable suggestions and comments.

ASELSAN A.Ş. for providing the necessary software and hardware. I extend my special thanks to *Mr. Vahit Özveren* for his support.

My friends *Haluk Erhan* from TUAF and *Bülent Sümer* from Tubitak-SAGE for their suggestions, and their precious brotherhood for all the time.

My dear family, my grandmother and my cousin *Evrım* for their smiling faces all the time with their endless support, patience and help during this thesis.

My precious *Mine Dođan*, for being a shining light with her worthy knowledge and intelligence, and for being a little child to remind me the beauty of life.

TABLE OF CONTENTS

PLAGIARISM	iii
ABSTRACT	iv
ÖZ	vi
DEDICATON	viii
ACKNOWLEDGMENTS	ix
TABLE OF CONTENTS	x
LIST OF TABLES	xiii
LIST OF FIGURES	xiv
LIST OF SYMBOLS	xvii
CHAPTER	
1 INTRODUCTION	1
1.1 Overview	1
1.2 Historical Background of Store Separation Testing	3
1.3 Literature Survey	5
1.4 Thesis Scope and Outline	7
2 THEORETICAL BACKGROUND	10
2.1 Overview	10
2.2 CFD-FASTRAN Flow Solver	12
2.2.1 Governing Equations	12
2.2.2 Space and Time Discretization	13
2.2.3 Initial and Boundary Conditions	14
2.3 USAERO Panel Code	16
2.3.1 Governing Equations	16

	2.3.2	Wall Boundry Conditions	17
	2.3.3	Surface Pressure Calculation	17
	2.3.4	Wake Treatment	18
3		FLOW SOLVER	19
	3.1	Overview	19
	3.2	Geometry Creation	20
	3.3	Structured Grid Generation	20
	3.4	CHIMERA Methodology	21
	3.4.1	Searching Process	23
	3.4.2	Hole-Cutting Process	23
	3.4.3	Interpolation Algorithm	25
	3.4.4	Setup and Application	25
	3.5	Parallel Execution	26
	3.5.1	Setup and Application Process	27
	3.6	Moving Body Module and 6DOF Equations	28
	3.7	Output Data	29
4		FLOW SOLVER VALIDATION TEST CASES	31
	4.1	Overview	31
	4.2	Chimera Validation Test Cases	32
	4.2.1	Store Alone Case	33
	4.2.2	Two Stores Side-by-Side Case	33
	4.3	Wing-Store Test Case	35
	4.4	Store Separation Test Case	39
	4.4.1	Configuration Geometry	39
	4.4.1.1	Wing Geometry	39
	4.4.1.2	Pylon Geometry	39
	4.4.1.3	Store Geometry	41
	4.4.2	Grids of the Configuration Geometry	42
	4.4.2.1	Wing-Pylon Domain	42
	4.4.2.2	Store Domain	43
	4.4.2.3	Overlapping Wing-Pylon and Store Grids	43
	4.4.3	Solution Parameters	45
	4.4.3.1	Initial and Boundary Conditions	45

	4.4.3.2	Solver Settings	46
	4.4.3.3	Convergence Criterion	47
	4.4.3.4	Chimera Parameters	48
	4.4.3.5	Transient Solution and Moving Body Parameters	49
	4.4.4	Separation Results of the Wing-Pylon-Store Test Case	51
	4.4.4.1	Linear and Angular Displacements of the Store	51
	4.4.4.2	Linear and Angular Velocities of the Store	53
	4.4.4.3	Forces Acting on the Store	54
	4.4.4.4	Separation Results Without Sting . .	56
5		RESULTS AND DISCUSSION	60
	5.1	Overview	60
	5.2	Configurations	60
	5.2.1	Wing-Pylon-Store Configuration	61
	5.2.1.1	Grids and Paneling	62
	5.2.1.2	Computations	62
	5.2.1.3	Smooth base-Sharp Cut base Force Comparisons	63
	5.2.2	F-16 Aircraft Configurations	64
	5.3	Results	66
	5.3.1	Wing-Pylon-Store Separation Results	66
	5.3.2	Fuel tank Separation Results from F-16 Aircraft	72
6		CONCLUDING REMARKS	76
		REFERENCES	81

LIST OF TABLES

TABLE

1.1	Evaluation Results for ACFD Challenge I	6
4.1	Memory need and CPU time comparisons of CFD-FASTRAN and Euler Solver[33]	36
4.2	Freestream Flow values for the validation test case	46
4.3	Solution parameters used in the Wing-Pylon-Store validation case[21]	50
5.1	Force coefficients on the store in its captive position, smooth and sharp-cut base comparisons, M=0.3	64
5.2	Moment coefficients on the store wrt. c.g. location in its captive position, smooth and sharp-cut base comparisons, M=0.3	64
5.3	Summary of the force and moment coefficients acting on the store in its captive carriage position, comparison of USAERO and CFD-FASTRAN solutions at M=0.3	72
5.4	Summary of the force and moment coefficients acting on the store in its captive carriage position, comparison of USAERO and CFD-FASTRAN solutions at M=0.6	72
5.5	Summary of the force and moment coefficients acting on the fuel tank in its captive carriage position right before separation, M=0.3	75

LIST OF FIGURES

FIGURES

1.1	Collision of a fueltank with the aircraft after its separation, pictures are taken from the movie of the flight test (ordered from left to right)	2
1.2	Picture from a store separation testing using Captive Trajectory System in Arnold Engineering Development Center, showing the instant positions of the store during separation	4
1.3	Relation between CFD, wind tunnel and flight tests	5
3.1	Steps of hole-cutting process for wall boundaries of wing in the store domain, sectional cut through store center in 3D	24
3.2	Selection of overlapping zones for the major zone using GUI	26
3.3	Coupling 6DOF calculations with the flow solver using Moving Body Module	29
4.1	Overlapping grids of store with the background grid	32
4.2	Hole-cut in the background domain for the store	33
4.3	Comparison of pressure coefficient distribution on the store with experimental data [32], one store configuration, $M=0.95$	34
4.4	Overlapping grids and hole-cutting through a section	34
4.5	Comparison of pressure coefficient distribution on the store with experimental data[32], two stores side-by-side configuration, $M=0.95$	35
4.6	Mesh view for the wing-store configuration [33]	36
4.7	Pressure distributions on the store and comparison to [33]	37
4.8	Lower and upper surface pressures of the wing, comparison of results with [33]	38
4.9	General Views of the Wing-Pylon-Store Configuration	40
4.10	Detailed Drawing of the Pylon	40
4.11	Detailed Drawing of the Store	41
4.12	Sectional cut at the root of the wing- pylon domain	42
4.13	Store grid topology through sectional cuts	43
4.14	Store domain, grids showing the outer chimera boundary	43
4.15	Overlapping store and wing- pylon domains	44
4.16	Grid around the store, between the store and the pylon	45
4.17	Comparison of the solutions with different grid resolutions to each other and to experimental data [8] using the pressure coefficient distribution on the store, wing- pylon- store case, $M=0.95$	46
4.18	Hole-cut in the store domain for the wing	47

4.19	First and second order spatial accuracy effect on the pressure distribution	48
4.20	Steady state solution residual graphs, wing-pylon-store test case .	48
4.21	Main steps taken in the solution of the store separation problem	49
4.22	Comparison of linear displacements of the store with the experimental data[8], wing-pylon-store validation case, M=0.95	51
4.23	Comparison of angular displacements of the store with the experimental data[8], wing-pylon-store validation case, M=0.95	52
4.24	Comparison of linear velocities of the store with the experimental data[21], wing-pylon-store validation case, M=0.95	53
4.25	Comparison of angular velocities of the store with the experimental data[8], wing-pylon-store validation case, M=0.95	54
4.26	Comparison of force coefficients of the store with the experimental data[8], wing-pylon-store validation case, M=0.95	55
4.27	Sting effect on the linear displacements of the store, wing-pylon-store validation case, M=0.95	56
4.28	Sting effect on the angular displacements of the store, wing-pylon-store validation case, M=0.95	57
4.29	Sting effect on angular velocities of the store, wing-pylon-store validation case, M=0.95	58
4.30	Sting effect on force coefficients acting on the store, wing-pylon-store validation case, M=0.95	58
5.1	Side view of wing-pylon-store configuration, sharp cut-base (left) and smooth-base (right)	61
5.2	Paneling and wake modeling of wing-pylon-store configuration for USAERO	63
5.3	F-16 Wing-Pylon-Store configuration	65
5.4	F-16 aircraft full configuration paneling and wake modeling	66
5.5	Linear displacements of the store after separation, comparison of CFD-FASTRAN and USAERO solutions at M=0.3	67
5.6	Linear displacements of the store after separation, comparison of CFD-FASTRAN and USAERO solutions at M=0.6	68
5.7	Angular displacements of the store with respect to its body axis after separation, comparison of CFD-FASTRAN and USAERO solutions at Mach 0.3	69
5.8	Angular displacements of the store with respect to its body axis after separation, comparison of CFD-FASTRAN and USAERO solutions at Mach 0.6	69
5.9	Pressure distribution on the store in its captive position, comparison of USAERO and CFD-FASTRAN solutions at M=0.3	70
5.10	Pressure distribution on the store in its captive position, comparison of USAERO and CFD-FASTRAN solutions at M=0.6	70
5.11	Time Histories of force coefficients acting on the store along its trajectory, comparison of USAERO and CFD-FASTRAN solutions at M=0.3, M=0.6	71
5.12	Linear displacements of the fueltank after separation, M=0.3 . . .	73

5.13	Angular displacements of the fuel tank after separation with respect to its body axis, $M=0.3$	74
5.14	Pressure distributions on the fuel tank in captive position, $M=0.3$	74
5.15	Time histories of force coefficients acting on the fuel tank along its trajectory, $M=0.3$	75

LIST OF SYMBOLS

ROMAN SYMBOLS		Q	Conserved state vector
b	Wing span	S	Surface
c	Chord length	t	Time
C_p	Pressure coefficient	u, v, w	Cartesian velocity components
$CFx,$	Force coefficient in x,	\vec{v}	Perturbation velocity
$CFy,$	in y,	\vec{v}_g	Volume surface velocity
CFz	in z direction	V	Volume
$CMx,$	Moment coefficient in x,	\vec{V}	Velocity vector
$CMy,$	in y,	V_b	Translational velocity of the body
CMz	in z direction	V_s	Surface point velocity
e_0	Total energy per unit volume	V_∞	Free stream velocity
\vec{F}	Resultant force vector	x, y, z	Cartesian coordinates
\vec{F}_c	Convective flux vector	X/L	Body axial location/body length
\vec{h}	Angular momentum vector		
I_{xx}	Roll moment of inertia		
I_{yy}	Pitch moment of inertia		
I_{zz}	Yaw moment of inertia		
L_2	Least-squares error norm		
m	mass		
M	Mach Number		
\vec{M}	Resultant moment vector		
\vec{n}	Unit normal vector to surface		
$n_x, n_y,$	Cartesian components		
n_z	of the surface unit normal		
P, Q, R	Roll, yaw, pitch angular rates		
p	Pressure		
		γ	Specific heat ratio
		ρ	Density
		τ	Non-dimensional time
		ϕ	Velocity potential
		$\phi,$	Roll,
		$\theta,$	Yaw,
		ψ	Pitch angular position of the store
		$\vec{\omega}$	Rotational velocity vector
		$\vec{\Omega}$	Rotational velocity vector

GREEK SYMBOLS

$\vec{\nabla}$	Gradient operator
∇^2	Laplacian operator

IGES Initial Graphics Exchange Specifications

IFM Influence Function Method

JDAM Joint Direct Attack Munition

MDICE Multi-Disciplinary Computing Environment

NURBS Non-Uniform Rational B-Splines

SUBSCRIPTS

<i>b</i>	Body
<i>c</i>	Cell adjacent to wall
<i>n</i>	Time step
<i>s</i>	Surface
<i>w</i>	Wall
∞	Freestream value

ACRONYMS

ACFD Applied Computational Fluid Dynamics

ADT Alternating Digital Tree

AEDC Arnold Engineering Development Center

BC Boundary Condition

CAD Computer Aided Design

CFD Computational Fluid Dynamics

CFDRC Computational Fluid Dynamics Research Cooperation

CFL Courant-Friedrichs-Lewy Number

CPU Central Processing Unit

CTS Captive Trajectory System

DOF Degree of Freedom

FDS Flux Difference Splitting

FVS Flux Vector Splitting

GUI Graphical User Interface

CHAPTER 1

INTRODUCTION

1.1 Overview

During World War I, a pilot or a bombardier could simply toss a bomb safely clear of his aircraft since the cockpit is open to air and no other mechanism rather than the pilot's hand was used for the ejection of the bomb. *Safe Separation* problem has been raised whenever the cockpit was enclosed and wide variety of bombs and stores with different kinds of ejection methods were started to be used in the aircraft industry [1].

Whenever a store is released in flight, it is supposed to clear the carrying aircraft without hitting or damaging it. In many situations, the precise point at which the store impacts on the ground is not of interest; the only requirement of the safe separation process is that the store does not collide with the aircraft. Pictures showing the collision of a 600 gallon fuel tank with an F-111/A aircraft after its separation are given in Figure 1.1.

Safe separation of a store from an aircraft is one of the major aerodynamic problems in the design and in the integration of a new store to an aircraft. Carriage loads and moments acting on the store should be correctly predicted in order to have an idea about its behavior after separation. It is difficult to predict the aircraft flowfield correctly, especially in the transonic regimes since the flowfield is highly dominated by shocks [2]. However, fighter aircrafts prefer to eject the

store flying at high speeds in order to escape from the dangerous area. Also, the interaction between the store and the pylon affects the attitude of the store after its release. Therefore, time consuming and costly wind-tunnel and flight tests are needed in order to obtain the necessary carriage and trajectory data. Since computational methods for the trajectory calculations give reliable data with less time and cost, they are used before and after the wind tunnel and flight tests to obtain the optimum integration and separation configurations for the store.



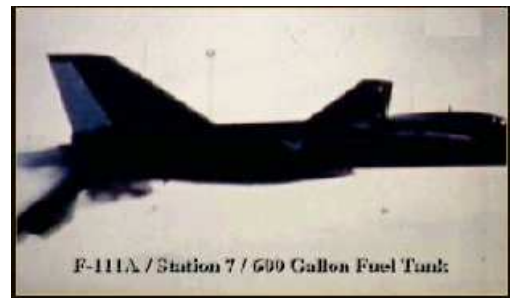
(a) Frame 1



(b) Frame 2



(c) Frame 3



(d) Frame 4

Figure 1.1: Collision of a fuel tank with the aircraft after its separation, pictures are taken from the movie of the flight test (ordered from left to right)

In this study, externally carried unpowered stores such as bombs and fuel tanks are concerned. The effect of the store on the airplane performance, structural loads on the configurations, aeroelastic effects and flutter will not be considered in the scope of this thesis study. Main focus on this subject is the motion of the store relative to the launch aircraft after it is released.

1.2 Historical Background of Store Separation Testing

Store separation tests were performed only using flight tests before 1960's. The test technique was called "hit or miss". In this technique, the stores are dropped from the aircraft at gradually increasing speeds. Since the critical flight conditions were not pre-defined, tests were performed until the store came close to or sometimes actually hit to the aircraft, which sometimes led to loss of aircraft [2].

Wind tunnel test techniques were improved during the 1960's; the *Captive Trajectory System (CTS)* method for the store separation wind tunnel testing was developed. The other method used in the store separation wind tunnel tests is *Grid Survey* technique.

In CTS technique, the airplane model is placed in the wind tunnel, and a store model is mounted on a separate sting balance. The forces on the store are measured by its balance, and send to the computer which calculates an increment of motion. This increment of motion in linear and angular directions is used to move the store to the next position along its trajectory by the sting support mechanism as shown in Figure 1.2. This method is considered as quasisteady unless the pressure measurements on the store are done in an unsteady way.

In grid survey technique, the airplane model mounted in a wind tunnel and a store model mounted on a sting is used as a probe to measure the aircraft interference flowfield rather than calculating the trajectory of the store. The measurements are performed at grid points in the aircraft flowfield. The measured data are forces and moments acting on the store. These data are stored in the form of interference influence coefficients. Static and dynamic characteristics of the store as a function of the angle of attack are also measured in a uniform stream. Calculation of the trajectory starts by putting the store to its initial point in the flowfield. The store-alone forces due to its motion and angle of attack are then added to the interference forces interpolated from the data bank and the resulting increment of motion is computed.

The wind tunnel store separation test results started to be using in planning of flight tests. But, since fairly small scale had to be used in the wind tunnel tests, flight test results did not match the wind tunnel predictions [2].

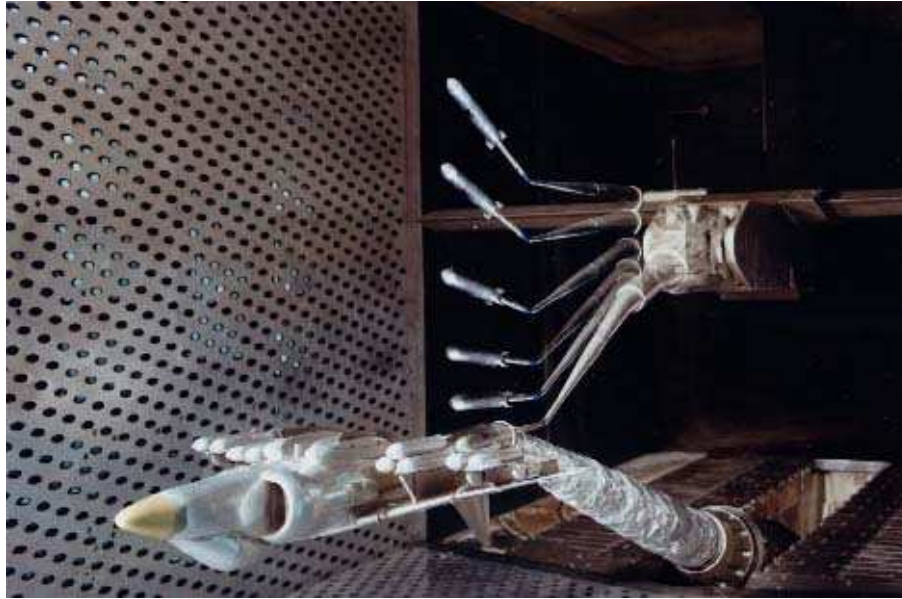


Figure 1.2: Picture from a store separation testing using Captive Trajectory System in Arnold Engineering Development Center, showing the instant positions of the store during separation

Development in Computational Techniques

One of the first computational result for a store in an aircraft flowfield was obtained by Cenko [3] in 1979. During this time period, *Influence Function Method (IFM)* [4], a semi-empirical way used to calculate the store loads in an aircraft flowfield was developed. This method is very similar to grid testing in wind tunnels. But the necessary data could not be still supplied to the flight test engineers for planning a successful test program.

Increase in the capabilities of computer resources directly increases the capabilities of the CFD tools. The linear methods are substituted with Euler and Navier/Stokes solutions. Moreover, using parallel processing, solution time advances by the number of processors used in the solution process.

Improvements in computational methods and wind tunnel test techniques by the 1990's caused to change the main idea of store separation analysis. The association among the CFD analysis, wind tunnel and flight tests was developed. The relation between these 3 legs of store separation analysis was given in Figure 1.3.

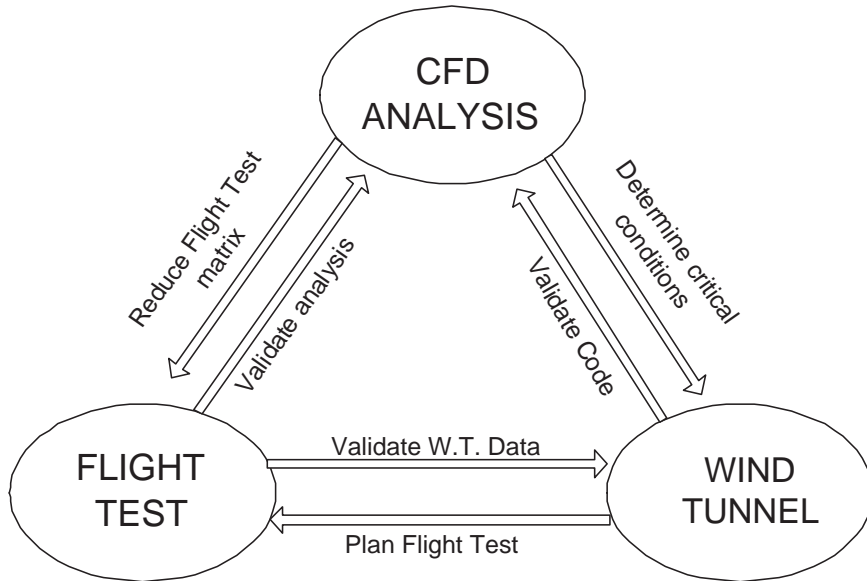


Figure 1.3: Relation between CFD, wind tunnel and flight tests

CFD techniques have showed their capability in the store separation analysis during the last decade of 20th century in three international CFD Challenges. The results of these challenges have shown that CFD can match the wind tunnel test data, and also the flight test results as well.

1.3 Literature Survey

The first store separation code used vortex lattice methods to model wing, and sources and doublets to model the fuselage. It was developed by Nielsen Engineering and Research Inc. (NEAR) [5] in 1971. The loads on the store are found by using the slender body theory. Later, PAN AIR code [3] was developed in 1979, allowing a higher order linear calculation for complex aircraft/store combination even at transonic speeds. PAN AIR code was coupled with IFM and used to find out the influence coefficients for the stores.

Advances in computer power and speed, and the solution techniques like Chimera [6] approach and unstructured grid techniques [7], true CFD calculations of store trajectories became practical. These improvements led to three CFD Challenges to determine how close CFD can come to matching wind tunnel and flight test data.

First challenge was held in 1992. The configuration was the generic Wing-

Pylon-Finned Store [8]. The wind tunnel tests were performed in Arnold Engineering Development Center (AEDC). Both Euler [9, 10] and thin layer Navier-Stokes solutions [11] were in good agreement with the test data. A full potential code, TranAir, [12] was also be able to get the similar results in a fraction of time than the higher order codes. Today, these test data are still used for the validation of CFD tools [13].

Second challenge was held in 1996 and named as Applied Computational Fluid Dynamics (ACFD) Challenge I. The configuration was the F-16/Generic Finned Store. Several codes were participated in this challenge. The fastest solution is obtained by TranAir [14] code in 2 weeks time. The most accurate result was obtained by OVERFLOW [15] solution, but this solution took 3 months of time. SPLITFLOW [16] provided 24 number of solutions in four months of time, some of which were in excellent agreement with the test data. The results were tabulated and given in Table 1.1.

Table 1.1: Evaluation Results for ACFD Challenge I

	TranAir	SPLITFLOW	USM3D	OVERFLOW
Solution time	2 weeks	1 month	1 month	3 months
Accuracy	3 rd place	2 nd place	3 rd place	1 st place
Number of Solutions	8	24	8	1

After the flight tests of this configuration were performed, it was seen that flight tests results did not match with the wind tunnel tests results.

The third CFD challenge was then announced as ACFD Challenge II. The configuration was F-18/C with MK-84 JDAM. Both the flight and wind tunnel test results were in good agreement with each other.

The results of several codes were in good agreement with the available test data. The participating companies and their code were CFD Research Corporation (CFDRC) with CFD-FASTRAN flow solver, Air Force Wright Research Laboratory with Cobalt flow solver and NAWSEP 6DOF motion module, Naval Air Warfare Center with SPLITFLOW, USM3D and PUMA, and Lockheed Martin with SPLITFLOW.

Cobalt flow solver is a parallel, implicit, unstructured-grid Euler/Navier Stokes code. Viscous solution of the F/A-18C aircraft solution consists of 6.62 million cells (half-model for symmetry) including 4 million for the boundary layer. The solution requires 10.1 GBytes of memory and the total 861 hours of CPU time was needed for the solution using IBM SP2 processors.

USM3D code is a tetrahedral cell-centered, finite volume Euler and Navier-Stokes flow solver. The viscous solution was run on a Cray C90 and required 315MW of memory and a total of 57.46 hours of CPU time.

SPLITFLOW is a cartesian-based, unstructured, adaptive Euler/Navier-Stokes solver. The viscous solution was run on a Cray C90 requiring 256 MW of memory and a total of 81.29 hours of CPU time.

Generally, the necessary accuracy was obtained, within the error range of wind tunnel and flight tests. The interesting result of this challenge is that both Euler and Navier/Stokes results gave similar results [17]. Comparisons of all the results obtained at ACFD Challenge II were presented in [17].

1.4 Thesis Scope and Outline

The purpose of this study is to demonstrate some of the capabilities of the computational prediction tools. Two separate computational tools are used; *CFD-FASTRAN*, an inviscid Euler solver with chimera overlapping grid technique and an unsteady panel method solver, *USAERO*, coupled with the integral boundary layer method. These codes are used to obtain the unsteady trajectory characteristics of a store released under subsonic flow conditions. The results are presented in terms of store trajectory, angular orientations, forces acting on the store in captive position and during separation process, and pressure distribution on the store in captive position.

CFD-FASTRAN is one of the codes that use implicit Euler/Navier-Stokes flow solver with chimera overlapping grid technique for relative body motion problems. This code is validated for the generic wing-pylon-store test case once and the results are presented in [18] and a similar technique of solution was further used to validate the simulation of a jettisoned aircraft canopy trajectory in the

same reference. Separation results of JDAM from an F-18 fighter aircraft are also published in [19].

USAERO, a time-stepping panel method coupled with a wake model and thin boundary layer assumption with Flight Path Integrator (FPI) module, is the other computational tool used for the present store separation problem. Since the modeling and the solution time of a panel code is considerably less than that of the Euler solutions, panel codes are frequently used as an engineering tool in achieving practical objectives [20].

Two different wing-pylon-store configurations are solved. The first one is the well-known generic wing-pylon-finned store test case [8]. It is solved with the *CFD-FASTRAN* solver at a Mach of 0.95. There are several reports that successfully predict the trajectory characteristics of this problem [21, 22, 23]. The results of the present computations are compared with the available experimental and computational data. It is observed that all of the major trends of the trajectory for this particular problem are captured with the present Euler solution technique [24].

The next case is the same generic wing-pylon-store configuration solved at two different Mach numbers of 0.3 and 0.6. Both codes are used to predict the c.g. location and the orientations of the store in its trajectory. As a final case, the separation of a fuel tank from an F-16 fighter aircraft's wing-pylon configuration and from a full F-16 aircraft configuration are also demonstrated with the use of *USAERO* unsteady panel code.

Unfortunately, no experimental data are available for Mach 0.3 and 0.6 cases of both the generic wing-pylon-store and the fuel tank separation from F-16 aircraft cases for comparison purposes. However, it is believed that the present results could be used to demonstrate the capabilities of both codes and their applicability for store separation problem [25].

Chapter 1 of the thesis gives a brief description of store separation problem. Historical background of store separation testing, wind-tunnel test techniques and developments in computational methods are introduced in this chapter. A literature survey about CFD tools used for store separation is also included.

Chapter 2 is about the theoretical background on which *CFD-FASTRAN* and *USAERO* package programs are based. Governing equations together with the boundary conditions modeling the fluid flow and their solution algorithms are briefly mentioned.

The capabilities of the Euler solver is explained in Chapter 3. Grid generation, Chimera overset grid methodology and its use in store separation problem, parallel processing, and 6-DOF motion model of *CFD-FASTRAN* are introduced.

Results of store alone and generic wing-pylon-store validation test cases with the present method, that is, Euler solution with chimera overset grid technique are given in Chapter 4.

Trajectory results of store separation from the generic wing-pylon-store and F-16 fighter aircraft cases are given in Chapter 5. First case is solved with both Euler and the unsteady panel codes. Similarities and differences in the results are discussed. Second case is solved in wing alone and full aircraft configurations using the unsteady panel code. Fuselage effect on the trajectory of the store after separation is investigated.

Chapter 6 presents the conclusions about the present study.

CHAPTER 2

THEORETICAL BACKGROUND

2.1 Overview

Computational fluid dynamics has the advantage of analyzing the separation phenomena with less time and cost than the experimental techniques. However, accuracy of the solution depends on the flow model. Solution of a flowfield around an aircraft with a turbulence modeling increases the accuracy of the solution by considering the viscosity effects. But the number of unknowns needed to be solved increases as well and are limited with the computational memory resources.

The challenge in separation analyses [2] is to decrease;

- man/hour required for modeling the problem,
- time required to obtain a solution,

and to increase

- accuracy of the solution

Modeling of the problem starts by importing the geometry from a CAD program, continues with the construction of the computational domain or surface paneling, and finalized by the start of the solution process. Time and man power required for modeling depends not only on how much the man is skilled, but also on the grid type that is used. For panel codes, only surface meshing is required. For Euler solutions, structured, unstructured or hybrid grids can be used to construct the solution domain. Navier/Stokes solutions require more attention to the

boundary layer around the wall boundaries. Therefore, time and skill required to model a separation problem increases with the accuracy of the solution.

Time required to obtain a solution depends on

- the number of the unknowns to be solved,
- the methodology used in the solution of unknowns
- and the processor speeds of the computer resources.

The number of unknowns to be solved increases from panel codes to Navier/Stokes solvers. Implicit methods converge faster than explicit methods. Increase in processor speeds and the memory capacity of a single computer make it possible to obtain solutions in shorter time.

Selection of the computational technique to be used in the solution of a store separation problem depends on the how much of the flow physics needs to be considered. If there is a strong interaction between the store and any part of the aircraft with shocks, solution can be obtained with Euler or Navier/Stokes solvers [26]. But higher order panel codes can also be used to get reasonably good results in such complex problems [20].

Euler and panel solvers are widely used in external flow analysis as well as store separation problems. Euler solvers are used instead of Navier/Stokes solvers when viscous effects are negligible. Therefore Euler solutions take the advantage of less memory requirements and less solution time when compared with Navier/Stokes solutions.

Panel codes are used in the solution of incompressible potential flows, where the flow is subsonic everywhere. Locally supersonic flows handled by Mach correction factors. Viscous effects can be added to the solution by boundary layer coupling.

In this study, Euler solutions are used for flows at high Mach numbers and where viscous effects can be neglected. For subsonic flows, unsteady panel code is preferred, due to its fast turn-out time to obtain the solutions. Viscous effects are also incorporated into the panel code calculations through an integral boundary layer coupling.

Following sections briefly describes the governing equations, and their discretization in space and in time, and the boundary conditions that are used by the Euler and the unsteady panel code.

2.2 CFD-FASTRAN Flow Solver

CFD-FASTRAN flow solver can handle a wide variety of physical phenomena including compressible, viscous/inviscid/laminar/turbulent flows with steady or time accurate calculations. Inviscid flow regime is governed by the Euler equations whereas for the viscous flow solutions, Navier-Stokes equations are solved. Steady state solutions take the advantage of numeric and advance the flow solution to a typically faster final answer at the cost of losing the time accuracy. Time accurate, unsteady solutions are required for the solution of transient flows such as moving bodies.

Finite volume approach is used for the numerical integration of the discretized governing equations, in which the flow domain is divided into discrete volumes. Governing equations are solved for each cell and the flow information is stored at the cell center. The flow from one cell to the next is determined by evaluating the fluxes across the common faces. *CFD-FASTRAN* includes Roe's Flux Difference Splitting and Van Leer's Flux Vector Splitting schemes for the flux calculations. These schemes are spatially first order accurate and several slope limiters are provided in *CFD-FASTRAN* which increases the spatial accuracy of the flux schemes to second or third order.

2.2.1 Governing Equations

The fluid motion is governed by the time dependent Euler equations for an ideal gas which expresses the conservation of mass, momentum and energy for a compressible inviscid non-conducting adiabatic fluid in the absence of external forces. The classical Euler equations are transformed for moving or deforming volumes by Leibnitz's Theorem. Conservation equations for an inviscid flow can be manipulated such that,

$$\frac{d}{dt} \int_V \mathbf{Q} dV + \int_S (\vec{F}_c - \mathbf{Q} \vec{v}_g) \cdot \vec{n} dS = 0 \quad (2.1)$$

where

$$\mathbf{Q} = \begin{pmatrix} \rho \\ \rho u \\ \rho v \\ \rho w \\ e_0 \end{pmatrix} \quad \vec{F}_c \cdot \vec{n} = \vec{V} \cdot \vec{n} \begin{pmatrix} \rho \\ \rho u \\ \rho v \\ \rho w \\ e_0 + p \end{pmatrix} + p \begin{pmatrix} 0 \\ n_x \\ n_y \\ n_z \\ 0 \end{pmatrix} \quad (2.2)$$

\vec{v}_g is the volume surface velocity and it is taken as zero for non-moving body problems. \vec{n} is the unit vector normal to the control surface and n_x , n_y and n_z are the cartesian components of the surface unit normal.

These equations are closed by the equation of state, which for an ideal gas is given by;

$$p = (\gamma - 1) \left(e_0 - \frac{1}{2} \rho |\vec{V}|^2 \right) \quad (2.3)$$

where γ is the ration of specific heats and its value is 1.4 for air.

Equation 2.1 states that the time rate of change of the state vector \mathbf{Q} within the control volume V is balanced with the net convective flux \vec{F}_c across the faces of the volume.

2.2.2 Space and Time Discretization

The flux vector and the flux jacobians are evaluated using the idea of upwind schemes. There are two upwinding flux schemes available in *CFD-FASTRAN*. The first scheme is based on Van Leer's scheme and is considered to be a flux vector splitting algorithm. Splitting the flux vector using this method make the flux functions continuously differentiable at sonic and stagnation points. The other approach is based on Roe's approximate Riemann solver and is considered as a flux difference scheme.

Roe's scheme is considered to be non-monotone, which means that erroneous extrema may be introduced into the flow solution, such as expansion shocks. This difficulty can be removed by specifying entropy fix to increase the numerical dissipation. On the other hand, Van Leer's scheme is considered to be monotone which means that dispersion (numerical oscillation) is unlikely to occur within a flow near a strong gradient, such as a shock. However, Van Leer's scheme is more dissipative than Roe's scheme in boundary layers which may cause if viscous effects are highly important. Van Leer's scheme's dissipative effects also cause it to be typically more robust than Roe's scheme.

First order spatial accuracy is not suitable for many aerodynamic simulations, especially if the flow is shock dominated as in transonic flows. Since both flux schemes are first order spatially accurate, higher accuracy is obtained by using flux limiters. Min-mod and Van Leer limiters, which are used in the present calculations, provide second order spatial accuracy.

The solution for the discretized equation is achieved by a time marching algorithm. For steady flows, the time marching scheme is repeated until the residuals or the change in the solution variables fall below a tolerance level. The time marching scheme produces a time-accurate answer for a transient simulation. In steady calculations, local time stepping is used whereas a global time stepping is used for the time accurate solutions.

A full implicit scheme is used for the present calculations. This scheme is first order time accurate for the transient calculations. VanLeer's and Roe's flux schemes are both used and tested for the calculations. It has been observed that both methods give similar results in the present calculations.

2.2.3 Initial and Boundary Conditions

An initial condition is needed to start the solution process in all steady/unsteady simulations. During steady state simulations of external flow problems, initial conditions are only initial guesses and do not affect the final solution but the convergence speed. Freestream values are assigned as initial conditions in the entire domain. Unsteady, time accurate simulations are initialized by the steady

state solution of the same problem.

Inflow/Outflow BC is set at the farfield boundaries. This condition calculates the total pressure and the total temperature from the user specified pressure, temperature and velocities at the inflow boundaries. The velocity direction is set by the user and the magnitude is determined by extrapolation from the interior domain. Same condition behaves as the fixed static pressure at the outflow boundaries while the remaining flow variables are extrapolated from the interior to the exit plane.

CFD-FASTRAN-GUI applies the inviscid wall boundary condition at the wall face for Euler calculations. The surface is impermeable and the flow velocity must be tangent to the surface for non-moving walls. For moving walls, the surface wall velocity is non-zero. The pressure and the density values at the wall are taken from the cell adjacent to the wall and the velocities are calculated using the equations below.

$$\begin{aligned}
 \rho_w &= \rho_c \\
 u_w &= u_g + \begin{bmatrix} 1 - n_x n_x & -n_x n_y & -n_x n_z \\ -n_x n_y & 1 - n_y n_y & -n_y n_z \\ -n_x n_z & -n_y n_z & 1 - n_z n_z \end{bmatrix} \begin{bmatrix} u_c - u_g \\ v_c - v_g \\ w_c - w_g \end{bmatrix} \\
 v_w &= v_g + \\
 w_w &= w_g + \\
 p_w &= p_c
 \end{aligned} \tag{2.4}$$

Symmetry boundary conditions are used at the symmetry surfaces. The static pressure and the static temperature are extrapolated to the symmetry boundary from the interior. At the symmetry boundary, the velocity normal to the boundary is set to zero and for all variables the gradient normal to the boundary is taken as zero.

Overset boundary condition is used for the structured overlapping surfaces. This boundary condition informs *CFD-FASTRAN* that flow information must be interpolated from one grid to another at the selected boundary.

2.3 USAERO Panel Code

USAERO is a low order panel code, which uses a time-stepping approach in the calculation of non-dimensional surface pressure coefficient and wake convection. The surface of the model is discretized with quadrilateral panels.

The basis of the method is that, the surface singularity model which uses quadrilateral panels of uniformly distributed doublets and sources are calculated at each time step. The surface integrals in Green's theorem are evaluated in a piece wise manner over each panel to form panel influence coefficients. These are evaluated for each panel acting at the central control points on all the surface panels, thus forming a matrix of influence coefficients. Usually the source values are determined at the start of each time step according to the local velocity component normal to the panel surface. The doublet values are then solved using the matrix equations.

The tangential velocity at the solid surfaces of the configuration is obtained from the doublet gradient. The normal component is provided by the source value. Off-body velocity perturbations are evaluated by summing all doublet and source singularity contributions. These velocities are used for general flow field information as well as for wake point convection. The wakes grow with each time step, with new wake points being propagated from the wake-shedding lines, while all the previous wake points are convected at the local fluid velocity.

2.3.1 Governing Equations

For an inviscid, irrotational and incompressible flow, Laplace equation can be written as;

$$\nabla^2\phi = 0 \tag{2.5}$$

The convention adopted here is that the perturbation velocity, \vec{v} , is the negative gradient of ϕ ;

$$\vec{v} = -\vec{\nabla}\phi \tag{2.6}$$

Green's Theorem is applied in the solution procedure of Equation 2.5. The contributions for the velocity potential, ϕ_p , for a point P on the wetted side of

the surface, are assumed to be due to;

- a surface distribution of normal doublets
- a surface distribution of sources
- the vortex shedding along the wake.

The source distribution is determined applying the Neumann boundary condition specifying the resultant normal velocity at the wall boundary. As for the wake treatment, the wake vorticity effectively varies in time and space according to the local stretching or contraction of the wake sheet as the wake points convect at the local velocities. Once source distribution and vortex shedding is known, doublet distribution along the surface is computed through the solution of Eqn. 2.5. Finally, perturbation velocity \vec{v} is calculated using Eqn. 2.6 knowing ϕ .

2.3.2 Wall Boundry Conditions

The condition to be satisfied on the wall boundary is that the normal component of the velocity to the wall equals to zero unless it is specified with an inflow/outflow normal velocity definition and/or boundary layer displacement effect. The normal component of the panel velocity includes the perturbation velocity from Equation 2.6, and the surface velocity relative to the undisturbed fluid. The surface velocity \vec{V}_s is defined as given in Equation 2.7.

$$\vec{V}_s = \vec{V}_b + \vec{\Omega} \times \vec{R} - \vec{V}_\infty \quad (2.7)$$

First term is coming from the translational velocity of the body, the second term is from the rotational velocity of the body and the last term is from the uniform flow.

2.3.3 Surface Pressure Calculation

The pressure coefficient is evaluated at each panel center using the Bernoulli equation for a moving frame given in Eqn. 2.8.

$$C_p = V_s^2 - V^2 + 2 \left(\frac{\delta\phi}{\delta\tau} \right) \quad (2.8)$$

V_s is the surface point velocity and V is the total fluid velocity relative to the surface point. The third term in the equation is evaluated by using simple differencing relative to the previous time step.

2.3.4 Wake Treatment

There is only one wake type to be used in *USAERO*, which convects with the local flow velocity. Internal treatment to the wake type is done automatically by the code through the boundary condition at the separation line. Also the jump in total pressure across a closed vortex-tube wake (jets or separation wake) is obtained automatically through the $\delta\phi/\delta\tau$ term in the pressure equation. In addition, this jump in total pressure is sensed automatically by any object enclosed by the tube.

CHAPTER 3

FLOW SOLVER

3.1 Overview

CFD-FASTRAN flow solver is a CFD package tool which includes its own pre and post-processors, *CFD-GEOM* and *CFD-VIEW*, respectively. *CFD-GEOM* is used in the creation of the geometry from points, lines, curves and surfaces. The same pre-processor is used for the generation of the structured grid. Chimera grids are created independently from each other using *CFD-GEOM*. Merging and overlapping the chimera grids are accomplished by a simple cut-paste technique. Hole-cutting process is performed automatically by the code during the solution state.

Parallel execution capability is applicable using both structured and unstructured grids and available only in Linux operating systems. *CFD-FASTRAN* uses a domain decomposition method based on multi-block approach in structured grids. In this decomposition, each block or blocks is/are assigned to different processor(s). Therefore, in order to have equal load distribution on processors, the blocks must be on same size of order. 6DOF module is used in store separation applications. Necessary data is input by the user using the Graphical User Interface (GUI). Application of the 6DOF module starts by entering the origin coordinates of the new body coordinate system. The forces acting on the store is selected at this stage. Available force features are aerodynamic, point, thrust

and gravitational forces. If needed, any prescribed motion can be modelled using the module.

Following sections briefly describes these features used in the solution of a store separation problem in *CFD-FASTRAN*.

3.2 Geometry Creation

The entire grid used in the solution process is generated with the pre-processor of *CFD-FASTRAN*, which is called *CFD-GEOM*. This tool can be used to generate structured, unstructured and also hybrid grids. In this study, structured grid tools of *CFD-GEOM* are used since *CFD-FASTRAN* solver use the body motion capability with chimera overlapping structured grids only.

The surface definition of the geometries is also generated using the same pre-processor. Given airfoil section defined by points on the line segments can be imported to the *CFD-GEOM*. Scaling property is used to scale the non-dimensional chord to the real values in meters. The root section of the wing is extruded along the span using the extrusion property in order to create the wing surface geometry. The store geometry is created by revolving the boundary curve that defines the surface curvature, around its axis of rotation. Other properties such as split, project, trim, translate, rotate are also used in the creation of the related geometries.

If necessary, any CAD file given in IGES or Plot3D format could also be imported by the pre-processor, which might speed up the geometry creation process.

In this study, the geometry of wing-pylon-store configuration is created using *CFD-GEOM*.

3.3 Structured Grid Generation

The structured grid generation process starts by defining the grid point number and its distribution on lines or curves. *Edge* creation option is used for this purpose. *CFD-GEOM* supports uniform, exponential and hyperbolic tangent grid point distribution along edges. Rectangular surface mesh of interest is defined

by three or four edges using *face* creation option. Revolving an edge around its axis of rotation can be used to create surface mesh of a circular body. Any face grid created can be projected exactly onto any NURBS surface set by projection. The projection algorithm projects the grid points to the nearest location on the NURBS surface to that grid point.

Six face sets combine to form a *block*. A block can be constructed manually by specifying six face sets that comprise the Imin, Imax, Jmin, Jmax, Kmin, Kmax sides of the block or by extruding a face. Creating a block means constructing the computational domain.

It is difficult to create the computational domain for complex geometries using single block. Therefore, a multi-zonal approach where the physical flow domain is divided into a number of geometrically simple sub-domains (zones) is highly favored over the single-zone counterpart. The multi-zonal approach also has the advantage that the mesh in a certain zone of the flow domain can be easily refined to accurately resolve shocks without modifying the meshes in the neighboring zones. Furthermore, multi zonal approach is needed for solving problems using multi-processing parallel computers in *CFD-FASTRAN*. In this study, structured grids with multi-block approach are used in creating the computational domains.

3.4 CHIMERA Methodology

There are two different multi-zonal algorithms depending on whether zonal boundaries exactly match or arbitrarily intersect each other. The former is named *patched* grid approach and the latter the *Overset* grid (Chimera) approach. In this study, both approaches are used.

In Chimera, overset grids can move relative to each other without disturbing the grids in other zones. Since different zones are not required to align with each other, zonal grids can then be produced completely independently.

Some advantages and disadvantages of the patched and overset grid algorithms are summarized below [27]:

Patched grid scheme

- Fully conservative

- Interpolation from one zone to another zone is unnecessary
- Zonal interfaces need perfect match

Overset grid scheme

- Arbitrary boundary interface matches
- Grids can move relative to each other
- Zonal boundary treatment is not fully conservative
- Two-way interpolations are required

CFD-FASTRAN-GUI uses non-conservative Chimera scheme since interpolations are used between grids to exchange information. In non-conservative Chimera approach, sub domains communicate by exchange of boundary information. The boundary data is obtained from interpolation of dependent variables. If the interpolation is done properly, the overall algorithm can achieve the same order of accuracy as the interior numerical algorithm. Since the interpolation is non-conservative, errors in the solution (conservative quantities) are usually the same order as that of the truncation errors of the numerical scheme. The errors are usually negligible in smooth regions and can be large in regions with discontinuities [28].

The original (non-conservative) and conservative interface algorithms for overlapped (Chimera) grids were evaluated in [29]. The conservative Chimera [30] was shown to possess superior conservative properties, faster convergence characteristics, and better shock capturing capabilities, especially for slow moving shocks. It is also shown that the original Chimera performed almost as well as the conservative Chimera for fast, strong shock waves [29].

In this study, the original Chimera methodology is used for allowing the moving body calculations. The computational domain of the body itself is constructed using patched grid. The methodology behind Chimera approach and the basic steps involved in the flow solver are described in the following sections.

In the following sections, bookkeeping of chimera methodology, hole-cutting process and interpolation algorithms are discussed. Finally, setup procedure for using chimera methodology is explained briefly.

3.4.1 Searching Process

Chimera scheme used by *CFD-FASTRAN* can find out the overlapping cells of different domains automatically. This property involves frequent searches over the cells in different zones. This searching process is optimized by an *Alternating Digital Tree* (ADT) [31]. AD tree disseminates the cells of a grid in a tree based structure, based on certain data such as the coordinates of cell centroid and the coordinates of bounding box for a cell which is a point in 6D space [31].

3.4.2 Hole-Cutting Process

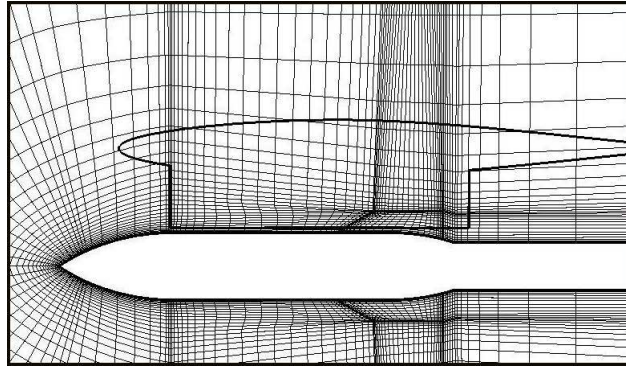
Hole-cutting is the process of blanking the cells in each zone that overlap with a wall boundary from another zone overset. Identification of the chimera-boundary cells, which are used to interpolate the flow variables from one zone to the other overlapping zones are also performed in this stage.

Major Zone is referred to the zone in which cells are blanked and *Minor Zone* is the zone which contains the wall boundary.

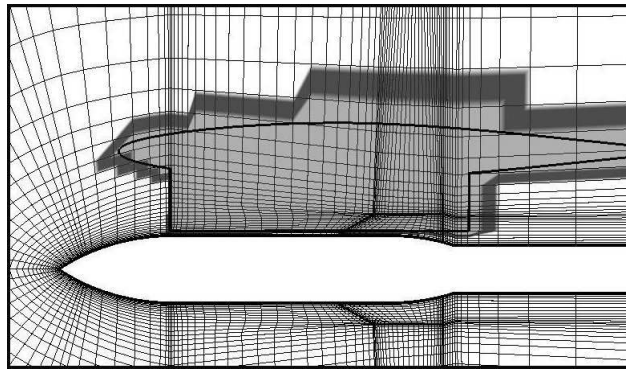
If there is wall a boundary in both overlapping zones, each zone is a major and a minor zone at the same time. The cells in the major zone that intersects wall boundary faces of the minor zone are first identified. This procedure is performed using the AD tree.

If the edge intersects a wall boundary, then the point at which they intersect is found. Next step is to find out if the nodes of the edge are inside or outside the wall boundary. The cell is marked as *cut-cell* if one of the edge nodes is outside the wall boundary while the other is inside.

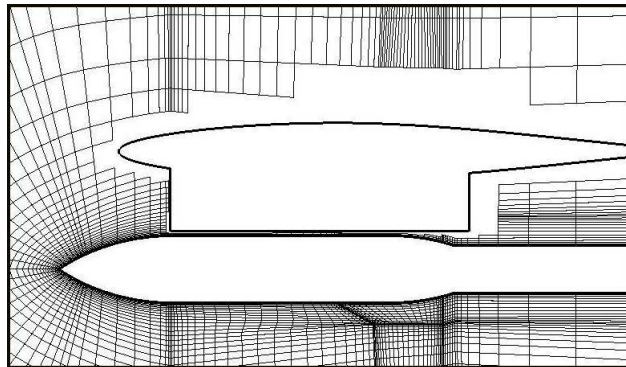
After determining the cut-cells, the nodes of the major zone that lie inside the blanket of these cut-cells are marked. These cells are blanked-out in the major zone. The region of blanked cells, inclusive of the cut-cells, is referred as *chimera hole*. The cells of the major zone surrounding the chimera-hole are marked as *chimera-boundary cells*. The solution is interpolated to these chimera boundary cells from the underlying *donor cells* in the minor zone. The mathematical expressions for this search process are given in Ref. [31].



(a) Overlapping wall boundaries of the wing



(b) Chimera hole (grey color), buffer layer (bold grey)



(c) Hole in the store domain

Figure 3.1: Steps of hole-cutting process for wall boundaries of wing in the store domain, sectional cut through store center in 3D

Buffer layer is an additional layer of blanked-cells added to the chimera-hole. If more than one buffer layer is used, the interpolation of flow variables to the major zone is performed using the cells which are number of buffer layer times away from the wall boundary of the minor zone. This prevents the major zone

from receiving flow information too close to the wall surface.

In order to perform an interpolation using more than one cell layer in the minor zone, additional *Fringe Layers* are used.

An application of hole-cutting for the wall boundaries of the wing in the store domain is given in Figure 3.1. Major zone is the store domain and minor zone is the wing-pylon domain for this application. First picture shows the overlapping wall boundaries of the wing-pylon in the store domain. In the second picture, the cell inside the wall boundaries of the wing-pylon which creates the chimera hole is in grey color. The bold grey boundary around the chimera hole is the buffer layer. Last picture shows the hole in the store domain created for the wing-pylon. The same procedure is applied for the store wall boundaries in the wing-pylon domain and a hole-cutting procedure is repeated.

3.4.3 Interpolation Algorithm

The identification of the minor cells that overlaps with the chimera boundary cells of the major zone follows the hole-cutting algorithm. ADT is used for this search process. A donor cell is identified as the cell in the minor zone which overlaps the chimera boundary cells of the major zone.

The flow information that is stored in the cell-centers of the minor zone grid is disseminated to the nodes. The solution at the nodes of the donor is then trilinearly interpolated [31] to centroid of the chimera boundary cell.

An *orphan cell* is a chimera boundary cell that did not find a donor cell after the AD Tree had been searched for each minor zone. These cells are chimera boundary cells that reside in the chimera hole of another grid. Since there is no donor cell for an orphan cell, solutions are interpolated its neighbor cells. Orphans are typically generated when two bodies with wall boundaries are in close proximity to one another. In order to avoid orphan cells, the overlapping grid layers must be at least 5 grid cells.

3.4.4 Setup and Application

The Chimera methodology is activated from the GUI under *Problem Type* menu. The donor information for each zone is given to the solver using the *Define*

Chimera sub-menu under *Model Options* page. If a zone is not overlapping with any other zones, this is also declared to the solver. All of these information speeds up the identification process of the chimera boundary cells. If the geometry is too complex in order to identify if a zone is overlapping with another zone or not, all of the zones can be taken as candidate donor zone, excluding the ones that are in the same domain.

Chimera Stencil Search Cycles controls the chimera hole-cutting frequency. For steady problems hole-cutting is performed only once and the frequency is ignored. For unsteady time accurate problems, depending on the displacements and time step size, this frequency is chosen between 10 and 20. In this study, this value is taken as 10. Therefore after every 10 time steps, solver searches for new overlapping cells and updates the chimera boundary lists. Appearance of the overlapping zone selection using GUI is given in Figure 3.2

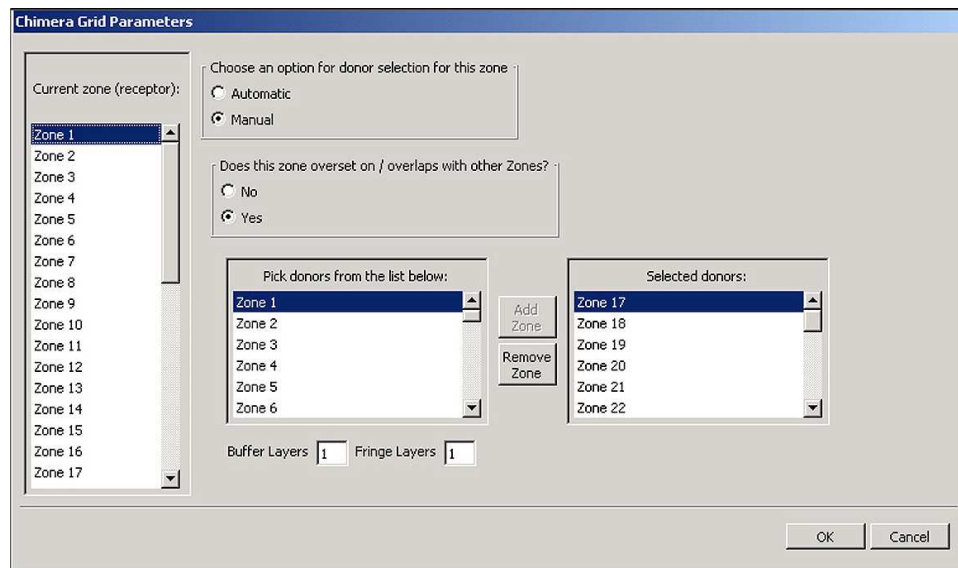


Figure 3.2: Selection of overlapping zones for the major zone using GUI

3.5 Parallel Execution

Main principle of parallel execution is to sub-divide the computational domain into many small volumes, which are solved by different processors. Therefore the computational time required for a solution process decreases inversely pro-

portional to the number of processors used. The necessary coupling between the solutions in the different sub-domains is accomplished by appropriate transfers of data between the processors. The data transfer speed affects the computational time required for the solution. For example, the time required for a four processor job will always be more slightly more than $1/4^{th}$ of the time required for the same job to be solved by a single processor. The structured-grid solver uses the *Multi-Disciplinary Computing Environment* (MDICE) utility to accomplish the data transfers between the CPU's. MDICE is a library of functions, developed by CFDRC, for storing data in arrays or other data-structures and is used for transferring or interpolating this data between different, simultaneously-running, arbitrarily-different codes, and for synchronizing the necessary data copying and data transfer operations [31]. MDICE also has several capabilities related to automated chimera hole-cutting and interpolation.

The *CFD-FASTRAN* structured-grid solver does not break a domain into sub-domains automatically. The domain decomposition is performed by distributing the blocks (zones) to different processors. The number of processors that can be used is limited with the number of zones used to construct the computational domain. The blocks must be created nearly of the same size in order to obtain a well balanced, equal load distribution.

3.5.1 Setup and Application Process

Parallel execution setup can be done using the *CFD-FASTRAN-GUI*. The processors, which are going to be used in the parallel execution, are initially listed in the *fastran.hosts* file created under the home directory of the user. This file also includes the relative speeds of the processors. Using the GUI, under *parallel set up* menu, these names can be found out. The blocks are distributed by the GUI after the processors are chosen. This distribution is optimized for the best performance depending on the speed of the processors and the block sizes. However, user can redistribute the blocks to the processors manually. The first processor becomes the *master* of the cluster, which performs the merging of solution files at the end of the computations. If chimera overlapping grids are used for the

computations, the last processor is assigned as the *Chimera host*, which performs the chimera related applications only.

Initial registry of the parallel execution is done by execution of *mdicer* program in any of the nodes used in the computations. The registry name given out by the program after this execution is used for starting the *mdice daemons* at the other nodes of the cluster. The parallel solution is started from the command-line. The decomposed domains are merged automatically at the end of the solution process.

3.6 Moving Body Module and 6DOF Equations

One of the capabilities of *CFD-FASTRAN* solver that is used for this study is the moving body module. This module is used for unsteady and time accurate problems such as store separation. This capability requires the rigidity of the body and the grids of the moving body being structured type. The motion of the body can be determined by a six degree of freedom calculation or it can be prescribed by the user.

The six degree of freedom, 6DOF, routine is based on the fluid flow solution in *CFD-FASTRAN*. Pressures and shear stresses are used to determine forces and moments acting on the body. In turn, these forces and moments are used in the general equations of motion to calculate translational and rotational displacements of the body.

The equations of motion for a rigid body with constant mass and mass moments of inertia are solved in order to obtain the linear and angular velocities and the displacements of the body in a delta time step size. These equations are given below.

$$\vec{F} = m \frac{d\vec{v}}{dt} \quad (3.1)$$

$$\vec{M} = \frac{\partial \vec{h}}{\partial t} + \vec{\omega} \times \vec{h} \quad (3.2)$$

where m is the body mass, \vec{v} is the linear velocity of the center of gravity, \vec{h} is the angular momentum, $\vec{\omega}$ is angular velocity about the body's center of gravity.

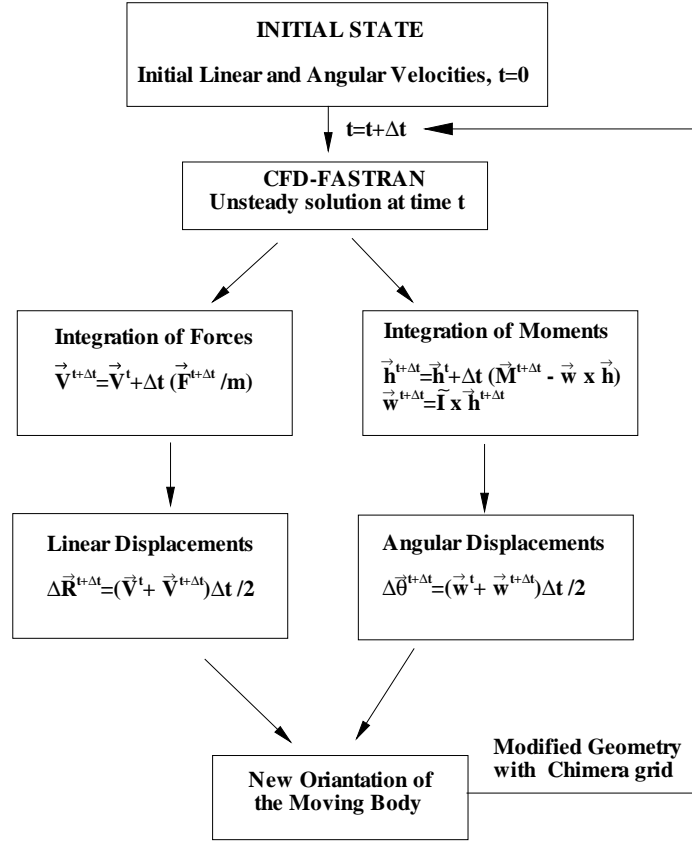


Figure 3.3: Coupling 6DOF calculations with the flow solver using Moving Body Module

The force equation Eqn.3.1 is in the inertial frame of reference. The momentum equation Eqn.3.2 is in the body fixed frame of reference. The moments of inertia are completely based on the body rotating about an axis passing through its center of gravity.

The main essential steps involved in these computations are given in Figure 3.3. This figure also summarizes the coupling steps of the flow solver with the 6DOF module.

3.7 Output Data

A file is created named ORPHAN, which prints out lists the cells which do not have valid interpolation stencils. The list includes the zone number, cell indices, and (x, y, z) location of the cell centroid.

The model.DYNA and model.DYNB files contain force and moment data created by each motion model. At each cycle, model.DYNA contains the individual forces in the x, y, and z directions. The individual forces printed in the file depend on the options selected in the GUI. The model.DYNB file lists the total forces in the x, y, and z directions for both inertial and body fixed axes. The total moments taken about the inertial (0, 0, 0) are also listed in inertial and body fixed axes. In model.KINA, the position, linear velocity and linear acceleration of the center of gravity of a motion model are printed out for each cycle. In model.KINB file, inertial angular displacement, body-fixed angular displacement, body-fixed angular velocity and body-fixed angular acceleration quantities are printed out for the motion model.

CHAPTER 4

FLOW SOLVER VALIDATION TEST CASES

4.1 Overview

In order to validate the *CFD-FASTRAN* flow solver capabilities, three test cases are solved and the results are compared with the available experimental and computational data.

The first test case studied is used to validate the chimera methodology of *CFD-FASTRAN*. The steady state solution a store carriage problem of a store alone and two stores side-by-side cases are used in this validation study. Wind tunnel tests are performed in the 4-ft transonic wind tunnels at Arnolds Engineering Development Center [32]. The non-dimensional pressure coefficient on the store at two different angular cuts is compared with the available test data. The results show that the Chimera hole-cutting process and the interpolation algorithm of the solver are working well even if there is an interaction between the two aerodynamic bodies.

The second case is the steady state solution of wing-store geometry. Wing and the store domains are individually created and chimera methodology is used to build up the flow domain. This configuration is solved using *CFD-FASTRAN* and compared with the results of an Euler solver [33]. Mach number is taken as 0.95. Chordwise pressure distributions on the wing and axial pressure distributions on the store at different angular cuts are compared with each other.

The third one is the validation of a store separation test case. The generic wing-pylon-store configuration is used for this study. The wind tunnel tests performed at Arnold Engineering Development Center’s (AEDC) 4-Foot Transonic Aerodynamic Wind Tunnel [8]. Test data are collected at store’s carriage position and at selected points along the trajectory of the store. Captive Trajectory System (CTS) simulated the motion of the store motion. The test data includes dimensionless pressure coefficient distribution on store, and force and moment coefficients acting on the store in its trajectory.

4.2 Chimera Validation Test Cases

The store used in the separation analysis is used to validate the chimera interpolation algorithm of *CFD-FASTRAN*. Two cases are considered for this study; store alone and two stores side by side. The experimental data are available in [32].

The background grid is a square domain; with edges 8 store lengths long each. The portion of the domain which overlaps with the store domain is finer in order to have adequate interpolation cells. In Figure 4.1, overlapping cells of the store domain with the background grid can be seen at a station cut along the store. In Figure 4.2, the hole-cut in the background grid for the store wall boundaries can be seen.

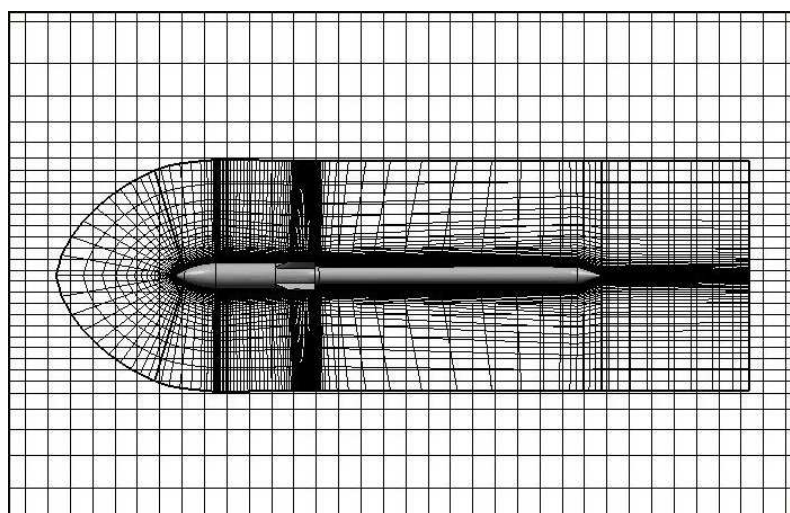


Figure 4.1: Overlapping grids of store with the background grid

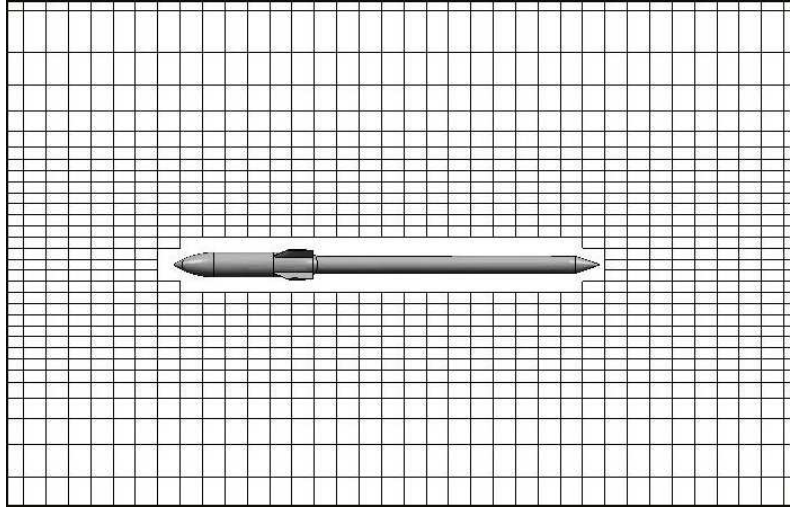


Figure 4.2: Hole-cut in the background domain for the store

The data was obtained in the 4-ft transonic wind tunnel at Arnold Engineering Development Center, Tullahoma, Tennessee[32]. The finned body is arranged in one, and two body combinations. In the two body configuration, the distance between the two bodies is 1.8 diameters of the store. Present calculations are performed at a Mach 0.95. Surface pressure distribution at an angular cut is compared with the experimental data available.

4.2.1 Store Alone Case

The first case is the store alone test case. The flow Mach number is 0.95. The solution is obtained by using VanLeer's flux vector splitting scheme. Higher accuracy is obtained by using VanLeer limiter. The non-dimensional pressure coefficient C_p distribution on the store at $\phi = 265^\circ$ angular cut is compared with the available experimental data in Figure 4.3. The Phi angle is measured clockwise when looking from upstream of the store and when the wing is at pilot's left shoulder. Present results show a good agreement with the experimental data. *CFD-FASTRAN* Euler solver overexpands before and overcompress after the shock since the viscous effects are neglected.

4.2.2 Two Stores Side-by-Side Case

The second test case is the two stores side-by-side configuration. This configuration is used to test the interpolation algorithm of the flow solver when there is a

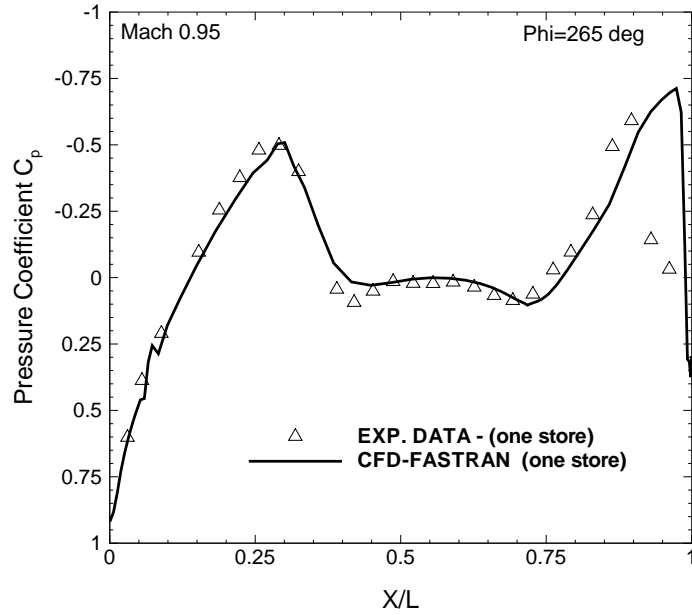


Figure 4.3: Comparison of pressure coefficient distribution on the store with experimental data [32], one store configuration, $M=0.95$

strong interaction between two wall boundaries. The distance between the stores is 1.8 diameters of the store body. The interpolation between the two domains and the background grid is realized by using the chimera boundary cells. A cut through the fins shows the overlapping grids of the two stores in Figure 4.4.

The non-dimensional pressure coefficient C_p distribution on the right store while looking from upstream at $\phi = 265^\circ$ angular cut is compared with the available experimental data in Figure 4.5. It is expected that the flow accelerates between the two bodies, as it is identified by the increase in expansion peaks. Also

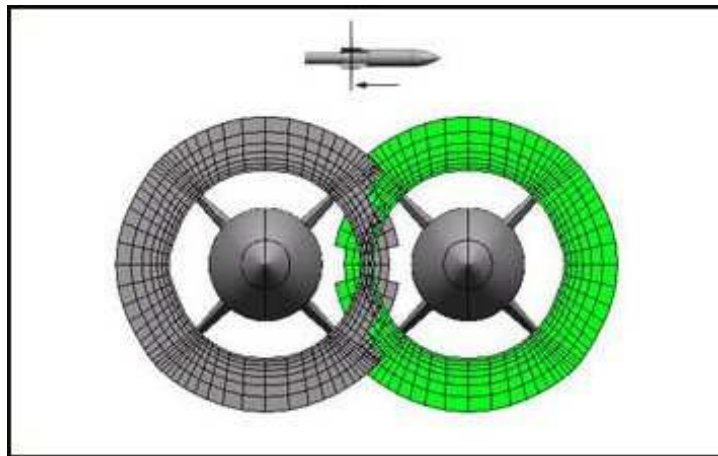


Figure 4.4: Overlapping grids and hole-cutting through a section

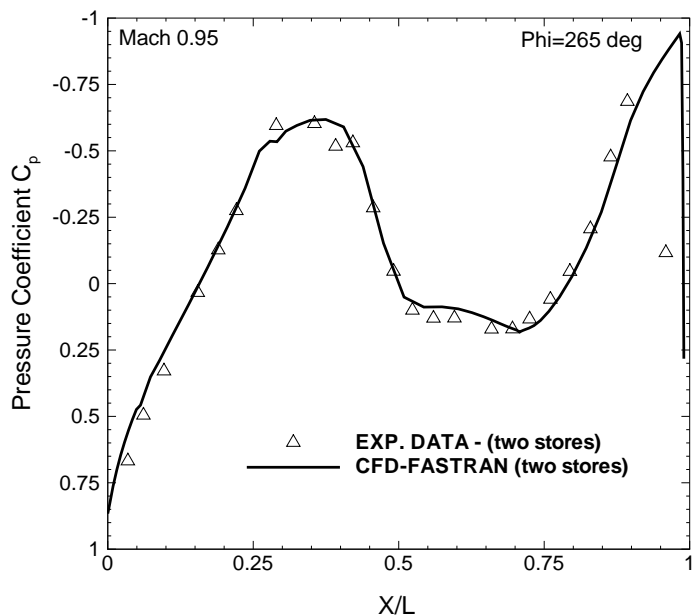


Figure 4.5: Comparison of pressure coefficient distribution on the store with experimental data[32], two stores side-by-side configuration, $M=0.95$

expansion regions increase in size, results the shocks moving downstream. Euler code overexpands before and overcompresses after the shock at the fin region due to viscous effects.

The coherence between the present results and the experimental data shows that the chimera scheme used in *CFD-FASTRAN* solver can also be used in the flow regimes where there is strong interaction between the aerodynamic bodies.

4.3 Wing-Store Test Case

Wing-Store test case is solved using the chimera methodology at Mach 0.95. The aim is to compare the results with another Euler code [33], which also uses the chimera technique for the solution. In order to eliminate the possible discrepancies due to grid generation, same grids are used in the solution of wing-store problem. Surface pressure distributions of the store at four different angular cuts and chordwise pressure distribution of wing at two different sections are compared with the results of [33].

The configuration geometry consists of a clipped delta wing and a simple store as shown in Figure 4.6. The store geometry is the same as used for the store alone test case in section 4.2.1, but the fins and the sting are not mounted

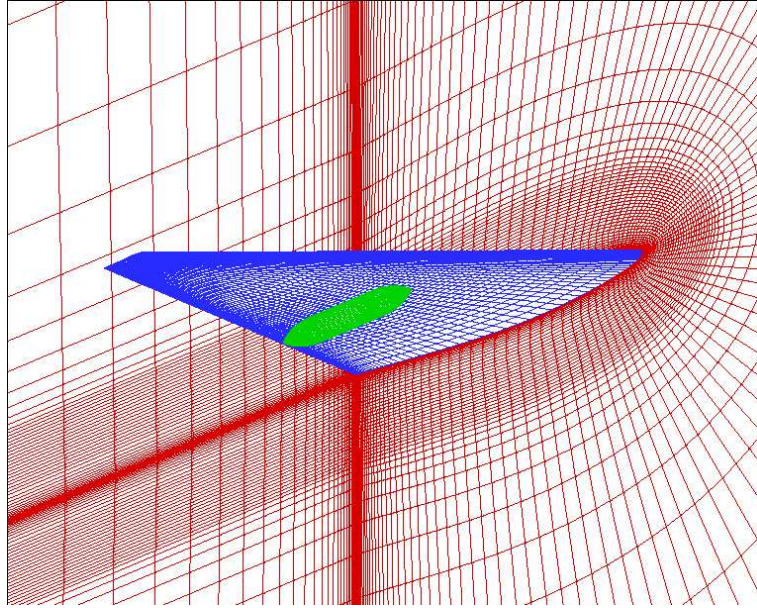


Figure 4.6: Mesh view for the wing-store configuration [33]

on the store for the ease of grid generation. The wing geometry is also used in the store separation test case and will be described in Section 4.4.1.1.

C-H type grid is used for the wing and a total number of 958,000 cells are produced for the solution domain. O type grid is used for the store. Total number of 124,000 cells are produced for the store domain. The wing grid is generated by *CFD-GEOM*, whereas the store grid is generated by the algebraic grid generation techniques [33].

An implicit time integration method with Van-Leer flux splitting scheme is used by *CFD-FASTRAN* solver. 900 iterations are needed to reach a converged solution. CFL number is taken as 20 for the calculations. The other Euler solver uses a finite difference method with an implicit time integration scheme. 6300 iterations are needed for a converged solution. Memory and CPU comparisons between the two solvers are given in Table 4.1

Table 4.1: Memory need and CPU time comparisons of CFD-FASTRAN and Euler Solver[33]

Solver	Processor	CPU time	Req. Mem.
CFD-FASTRAN	1	40 hrs.	936 MB
Euler Solver	2	20 hrs.	280 MB

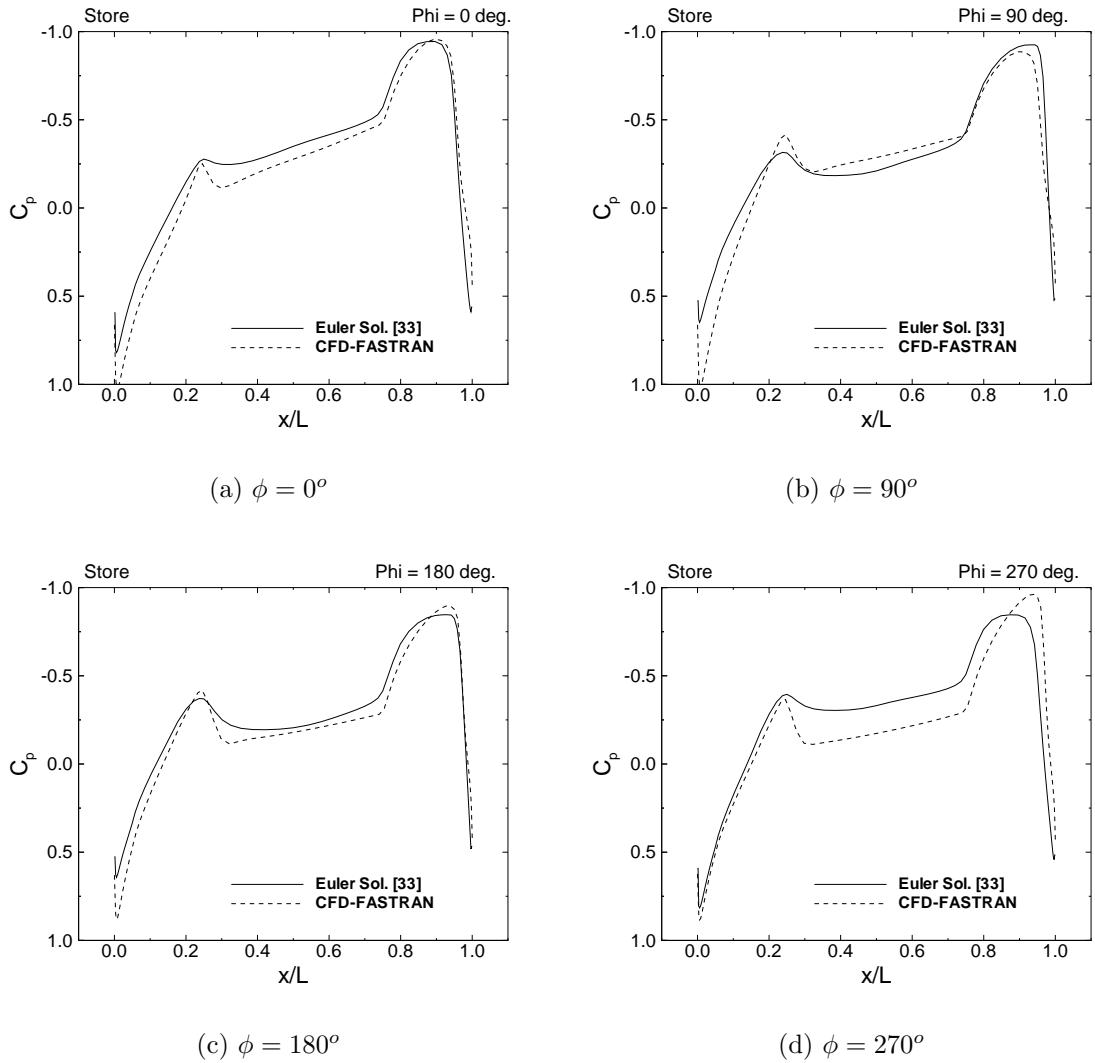


Figure 4.7: Pressure distributions on the store and comparison to [33]

The pressure distribution on the store along the axial direction at four different phi angles are given in Figure 4.7.

The pressure coefficient distributions obtained by the two codes are almost the same with small differences in the magnitudes. Smoother passages after the first shock are observed in the Euler code [33] solution results due to artificial viscosity effects. The far most location of the store from the wing, $\phi = 180^\circ$ angular cut has shown the best similarity between the two codes. At $x = 0.25$, both codes has shown the compression at all angles. But at $\phi = 0^\circ$ and $\phi = 270^\circ$ angular cuts, this compression has a higher strength in the results of *CFD-FASTRAN*.

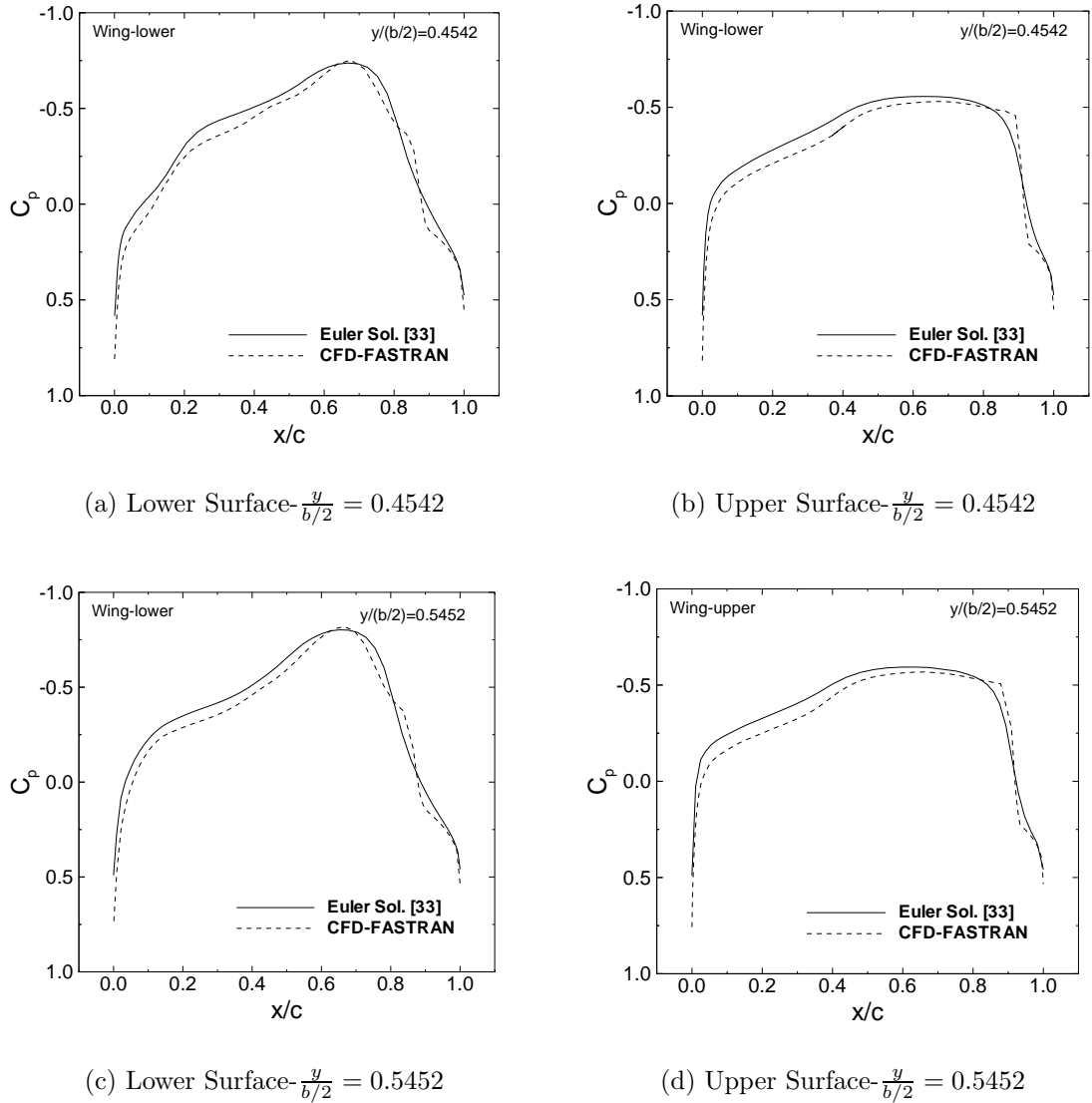


Figure 4.8: Lower and upper surface pressures of the wing, comparison of results with [33]

The chordwise pressure distribution on the lower and upper surface of the wing at two different sectional cuts are given in Figure 4.8. The results of both codes are again very similar to each other. However, *CFD-FASTRAN* results have sharp changes at the shock locations. The same dissipation effects of the Euler code has been seen at the store pressure distributions.

The same trends shown in the graphs and better resolutions in the shock locations are observed using *CFD-FASTRAN*. These results show that the flow solver and the chimera technique used in the solutions are applicable to use for wing-store configurations at high Mach numbers.

4.4 Store Separation Test Case

4.4.1 Configuration Geometry

The model geometry consists of a clipped delta wing with a 45° leading edge sweep, a pylon located at the mid span of the wing, and a store having four tail fins positioned in a cruciform style. The configuration geometry used in the wind tunnel tests is described in detail in the following sections [8]. The wind tunnel model is taken as 5% scale of full configuration as used in [21]. The dimensions given in figures are belonging to the geometry used in the computations. The geometry of the configuration is built up using the CAD properties of the pre-processor *CFD-GEOM*.

4.4.1.1 Wing Geometry

Wing profile is NACA64A010 airfoil section and is constant throughout the span. It has a form of clipped delta wing with a 45 degree leading edge sweep. Trailing edge has no sweep angle. The taper ratio is 0.133 and the root and the tip chords are 7.62 and 1.016 meters respectively. There is no twist and the half span of the wing is 6.604 meters. Detailed drawings of the wing and the coordinate system are given in Figure 4.9.

4.4.1.2 Pylon Geometry

The pylon has an ogive-flat plate-ogive cross section shape, which is closed at the leading and trailing edges by a symmetrical tangent-ogive shape. The width of the pylon is 0.149 meters, maximum between the flat plates. The radius of the ogive section is 0.635 meters and the length of the ogive section is 0.297 meters at both ends. The pylon is located at the midspan of the half wing. The leading edge location of the pylon is 0.3891 meters aft of the leading edge of the wing. The total length of the pylon is 2.286 meters. Detailed drawing of the pylon is given in Figure 4.10.

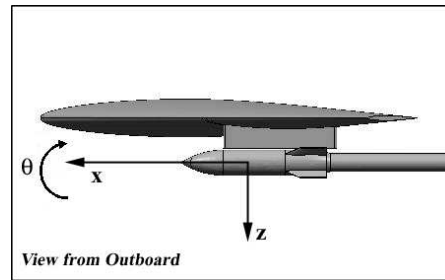
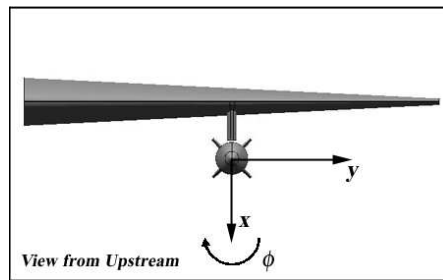
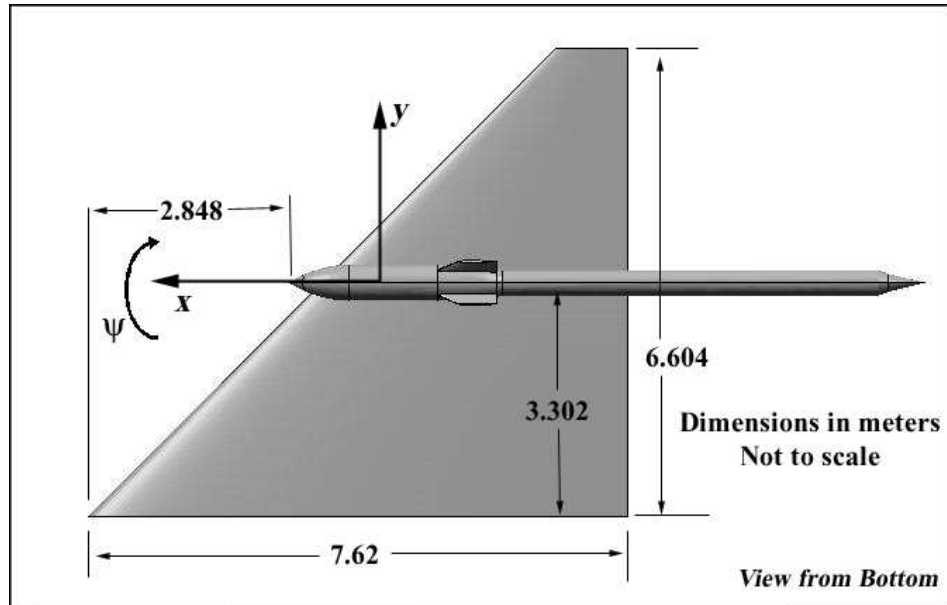


Figure 4.9: General Views of the Wing-Pylon-Store Configuration

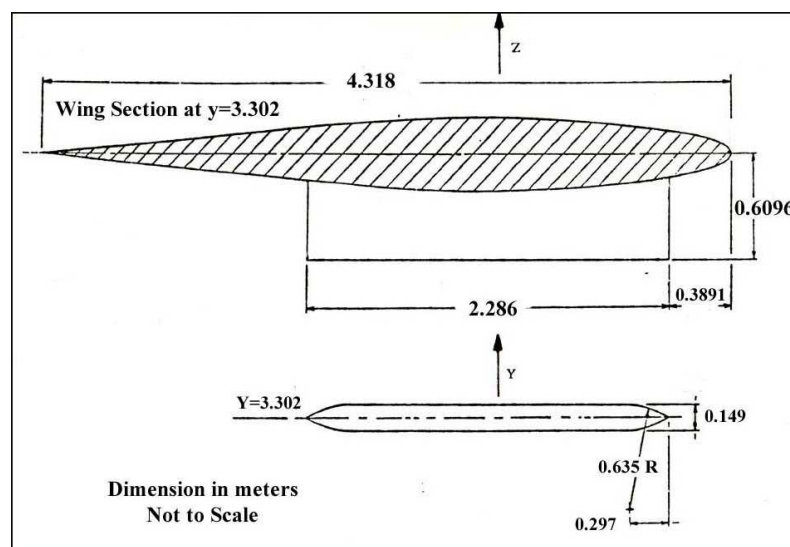


Figure 4.10: Detailed Drawing of the Pylon

4.4.1.3 Store Geometry

The store is a tangent-ogive cylinder at the forebody and the afterbody. Radius of the ogive is 1.5383 and length of each ogive is 0.8467 meters. Diameter of the store is 0.5081 meters. The store has four fins that are located at the tail side in a cruciform style. The fins are identical and they have a constant profile (NACA0008) throughout the fin span. Leading and trailing edge sweep angles of the fins are 60 and 0 degrees, respectively. Root chord length of the fins is 0.8467 meters and the tip chord length is 0.5388 meters. The fins are clipped to the store body. The store is located at the midspan of the wing at carriage position. There is a gap of 0.03556 meters between the store and the pylon. The store's nose is 0.8468 meters ahead of the pylon. Drawing of the store with dimensions is given in Figure 4.11. The position of the store under the wing is also given in Figure 4.9.

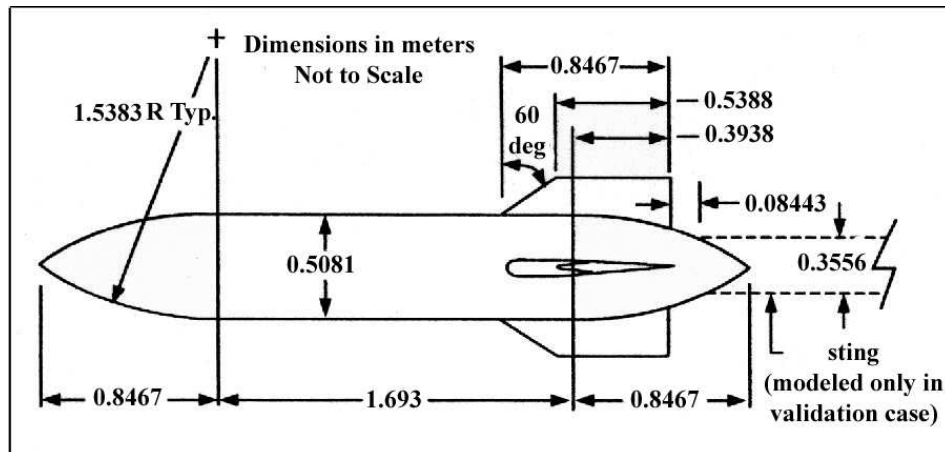


Figure 4.11: Detailed Drawing of the Store

For the sake of the physical coherence, the store is modeled with the sting mounted to it as it was used in the captive trajectory system experiments. Its main duty in the experiments is to hold the store at its location, and to move the store to its new location after the trajectory calculations are performed at each time step. However, since the existence of the sting in the wind tunnel experiments are influencing the pressure and the velocity field during its separation from the wing, the same configuration was modeled in the CFD analysis to have a one-to-one correspondence between the computations and the real tests.

There are two sting models used in the experiments; one for pressure measurements and the other for force measurements. The pressure model is used in the numerical calculations since the geometry of the force model is not available in references.

4.4.2 Grids of the Configuration Geometry

The pre-processor of *CFD-FASTRAN*, *CFD-GEOM*, is used for structural grid construction for all the configurations. The wing and the pylon are meshed together using a multi-block approach. For the moving body application, the store is meshed alone and is placed in the wing-pylon domain using the Chimera overlapping grid methodology.

4.4.2.1 Wing-Pylon Domain

Wing and the pylon are immersed in an H type structured grid using the multi-block approach. Whole domain is a rectangular box, where the far field boundaries are placed 7 root chords away in chord-wise direction and 5 root chords away in the span-wise direction. Total number of grids used for the wing-pylon domain is 807,000. Pylon surface is composed of 15x45 (spanwise) grid nodes and the wing upper surface is composed of 70 of chordwise x 63 of spanwise grid nodes. 23 blocks are used for this domain creation. A sectional cut at the root section of the wing-pylon domain is given in Figure 4.12 .

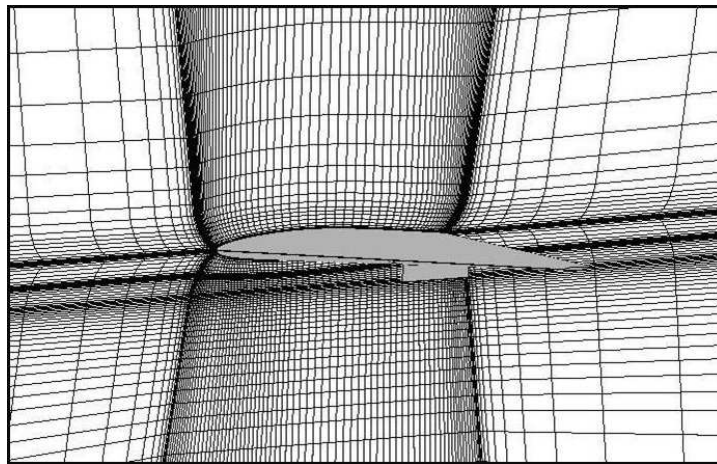


Figure 4.12: Sectional cut at the root of the wing-pylon domain

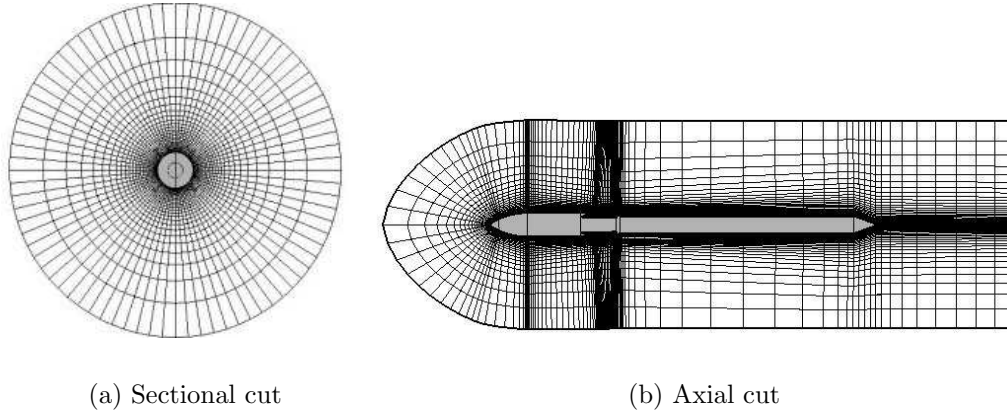


Figure 4.13: Store grid topology through sectional cuts

4.4.2.2 Store Domain

C type grid is used for the nose and H type grid is used around the fins. O type grid is used around the cylindrical body and the sting. The volume mesh is built up with 16 blocks having a total of 280,000 cells. Figure 4.13 shows the grid topology of the store through a sectional and an axial cut. Figure 4.14 shows the outer boundary of the store domain.

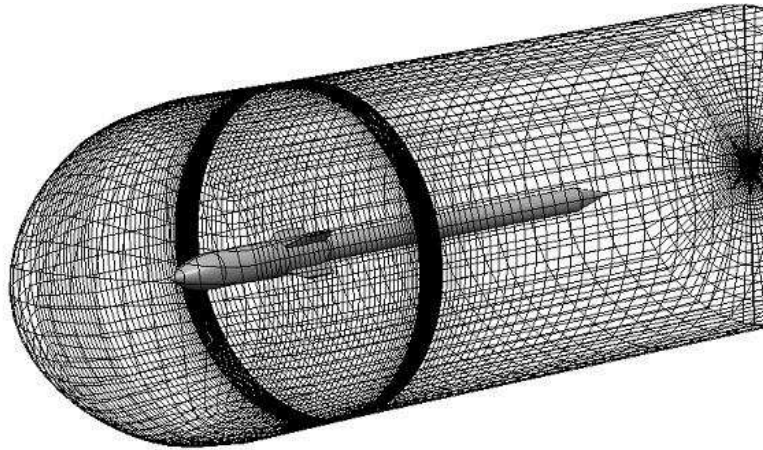


Figure 4.14: Store domain, grids showing the outer chimera boundary

4.4.2.3 Overlapping Wing-Pylon and Store Grids

Individually generated wing-pylon and the store multi-block domain grids are overlapped in order to have the real flow domain as shown in Figure 4.15. Dark black lines belong to the store domain. This process is simply performed by using

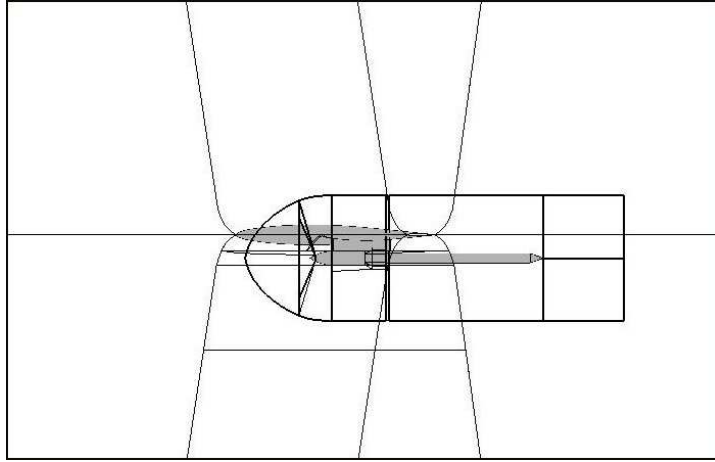


Figure 4.15: Overlapping store and wing-pylon domains

the "cut & paste" function in the *CFD-GEOM* pre-processor.

The most important part of the Chimera application is the control of overlapping grid density of two wall boundaries. The critical part of the geometry is the finite gap between the store and the pylon (Figure 4.16). The Chimera methodology in *CFD-FASTRAN* needs at least five overlapping cells between the two overlapping grids of the pylon and the store wall boundaries in order to perform the hole cutting process and the interpolation routine. Otherwise, cut-cells of wing-pylon domain blank out the wall boundaries of the pylon. This is the failure of the hole-cutting process. Due to this, wall-to-wall overlapping grids in *CFD-FASTRAN* are not applicable to chimera overlapping grid methodology. A small distance between the two wall boundaries must be available.

Therefore the grid node resolution under the bottom section of the pylon and near around the store body are controlled by the grid node distributions on the edges of structured faces. Two test files are created with coarse and fine grid resolutions around the store domain and under the pylon region. The grid resolution around the store domain after the hole cutting process is given in Figure 4.16 for both cases. The steady state solutions for these cases are obtained using second order VanLeer FVS and pressure distributions on the store at $\Phi = 5^\circ, 95^\circ, 185^\circ$ and 275° degree angular cuts are compared with the experimental data [8] in Figure 4.17.

The 5 degree Φ angle cut on the store corresponds to the region between

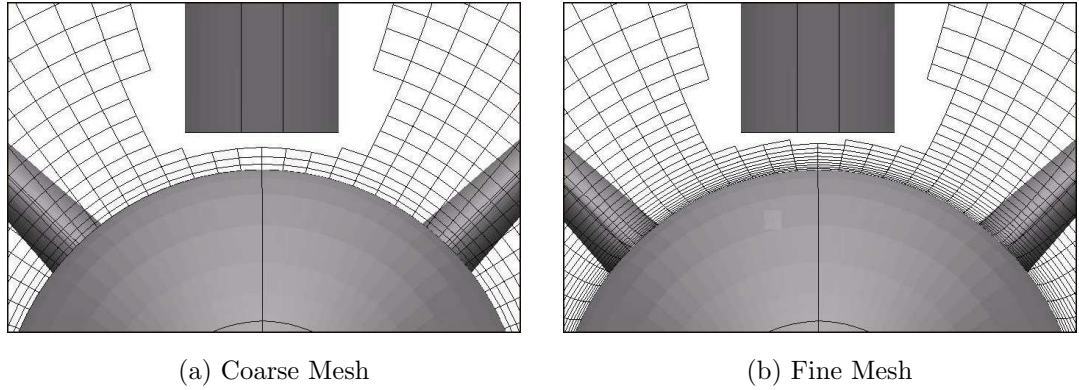


Figure 4.16: Grid around the store, between the store and the pylon

the pylon and the store where there is a significant interaction between two wall boundaries. Both coarse and fine meshes around the store and under the pylon solutions captures the compression due to pylon at $X/L = 0.25$. However, the expansion after this compression is only captured perfectly with the finer mesh distribution.

There are some discrepancies between the fine grid solutions and the available data due to inviscid nature of the solver. However, for all angular section cuts, the results are in better agreement with the data than the coarse mesh solutions.

The grid node distribution along the separation trajectory of the store under the wing is finer than the upper side of the wing. This is a guarantee for finding the donor cell for the chimera boundary cells of store domain and the wing domain.

4.4.3 Solution Parameters

This section describes the parameters which are used in the solution of the validation test case. These parameters are explained under the sections of initial and boundary conditions, solver settings, convergence criteria, chimera methodology, transient solution and moving body parameters in detail.

4.4.3.1 Initial and Boundary Conditions

All domains are initialized with the freestream values in steady solutions. These freestream velocity, pressure and temperature values are given in Table 4.2. These

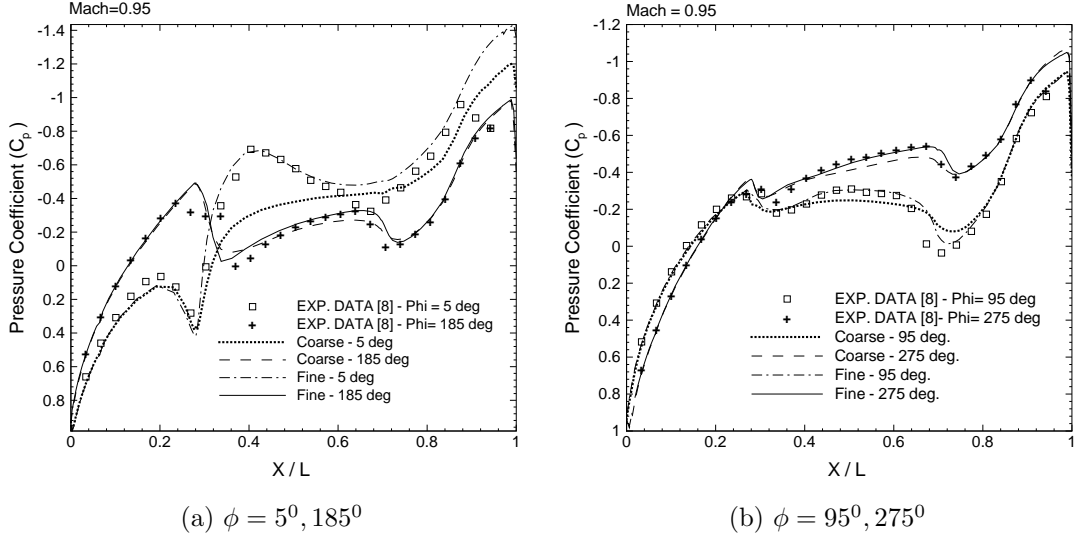


Figure 4.17: Comparison of the solutions with different grid resolutions to each other and to experimental data [8] using the pressure coefficient distribution on the store, wing-pylon-store case, $M=0.95$

Table 4.2: Freestream Flow values for the validation test case

Velocity	Pressure	Temperature
293 m/s	36040 N/m ²	236 K

values are calculated at 26000 ft pressure altitude for a Mach number of 0.95 [21]. Steady solution results are used as the initial condition for the transient solutions. Inflow/outflow boundary condition is given to the outer boundaries of the wing-pylon domain. Symmetry boundary condition is used for the symmetry plane.

Hole-cutting option is also activated for the symmetry boundary condition since some part of the store domain belonging to the sting overlaps with the symmetry plane during its trajectory. Chimera boundary condition is applied to the outer face of the store domain as shown in Figure 4.14. The hole-cut in the store domain for the wall boundaries of the wing-pylon is given in Figure 4.18.

4.4.3.2 Solver Settings

In the solutions, inviscid flow model and ideal gas assumption is used. Steady solution process starts using 1st order spatial accuracy using Roe's Flux Difference Scheme (FDS) for the flux computations. Point Jacobi implicit scheme is used for

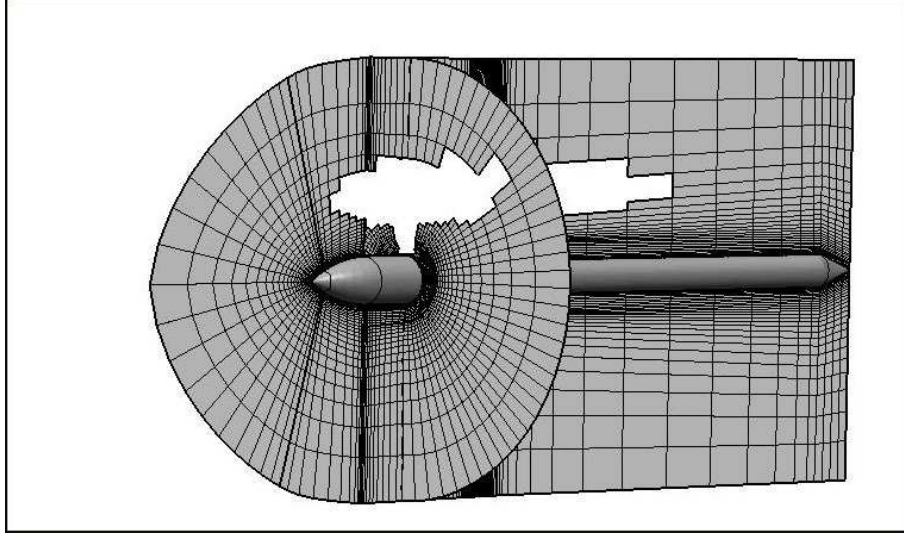


Figure 4.18: Hole-cut in the store domain for the wing

the time integration. Convergence in residuals for the 1st order spatial accuracy is obtained in 800 cycles, starts with a CFL number of 1 and increases to 20 in 100 cycles and then stays constant for the rest of the iterations. 2nd order spatial accuracy is obtained using minmod (1/r) limiter. 800 cycles are enough with a CFL number of 1 increasing to 20 in 100 cycles for convergence. Figure 4.19 shows the spatial accuracy effect on the pressure distribution at an angular cut of $\phi = 5^\circ$ on the store. If coarse mesh is used in the interpolation area, 2nd order spatial accuracy does not enough to get the correct resolution. Fine interpolation grid with 2nd order spatial accuracy shows the best coherence with the available experimental data [8].

4.4.3.3 Convergence Criterion

Convergence of the solution is monitored with L2 norm of the conserved variables. Generally for 3D applications, residuals decrease at most 2 orders of magnitude. Oscillations may appear after 2nd order spatial accuracy is used for the solutions. Therefore, aerodynamic force and moment cycle histories of the components are calculated at the wall boundaries and monitored during the solution. Steady state solution is said to be converged after the forces and moments stay constant. Residual history of density for a converged solution using both Roe's FDS and VanLeer's FVS schemes are given in Figure 4.20. Dissipative effect of VanLeer's

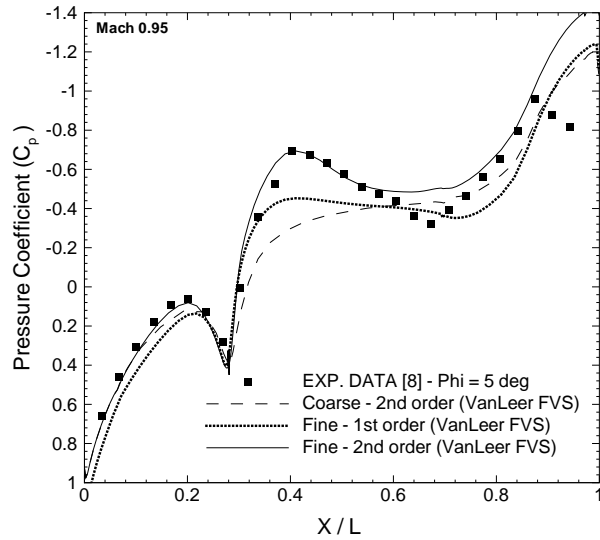


Figure 4.19: First and second order spatial accuracy effect on the pressure distribution

scheme results in less oscillation in residuals than Roe's scheme.

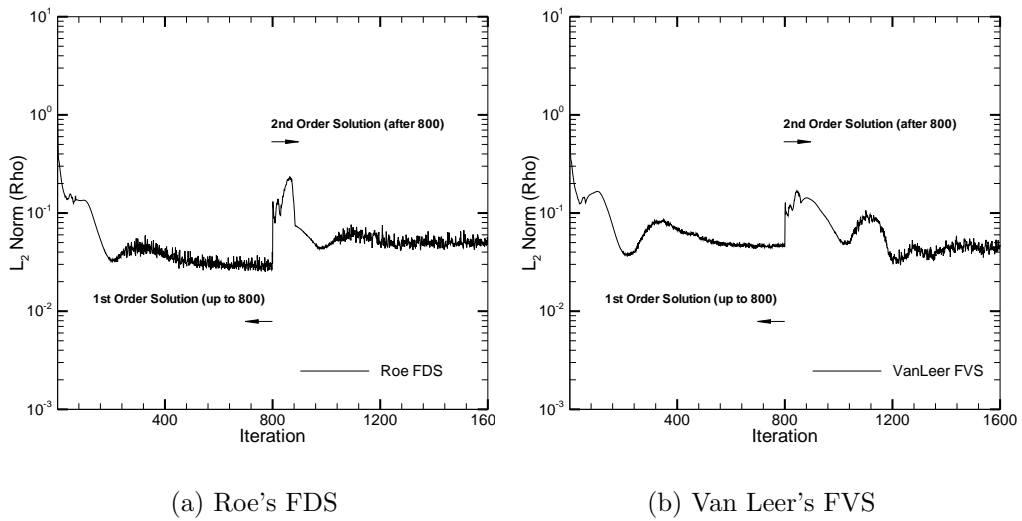


Figure 4.20: Steady state solution residual graphs, wing-pylon-store test case

4.4.3.4 Chimera Parameters

Chimera module is activated since this methodology is used for all overlapping structured grid solutions. All of the zones of the store computational domain are set to be the donor candidate of the wing-pylon domain and vice-versa. Number of buffer and fringe layers for all overlapping zones are taken as one.

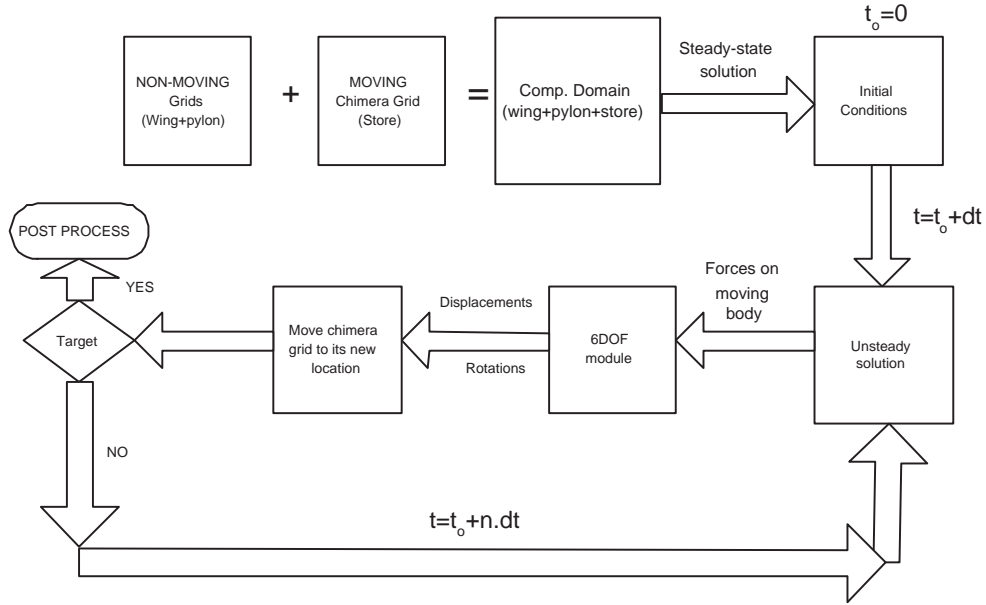


Figure 4.21: Main steps taken in the solution of the store separation problem

4.4.3.5 Transient Solution and Moving Body Parameters

Transient solutions are used for the trajectory calculations of the store after its separation from the wing. Figure 4.21 shows the placement of the transient solutions in the store separation problem.

Time step is calculated for each cell by the solver using the CFL number given as input parameter. The smallest time step is chosen and used as the global time step for the unsteady solutions. The corresponding time step for the given CFL number can be found from the output data. For the present calculations, a time step of 0.00005 is used as the Δt value. This time step is obtained using a CFL number of 7140.

Steady state solutions are assigned as the initial condition for the transient solutions. Since the local time stepping is used for the steady calculations, there is a passage of CFL number of 20 to a higher value of 7140, which is used. This transition is accomplished by carrying on the solutions using a global time stepping method after the steady solutions are converged. During these transient calculations, CFL number is increased from 20 to 7140 in 1000 cycles.

Moving Body module is activated using the GUI. Using motion models setup menu, necessary input parameters are given to the solver. First, body coordinate

Table 4.3: Solution parameters used in the Wing-Pylon-Store validation case[21]

Weight of the store	2000 <i>lb</i>
Center of gravity	4.65 <i>ft</i> aft of store nose
Aft ejector location	5.73 <i>ft</i> aft of store nose
Aft ejector force	9600 <i>lb</i>
Forward ejector location	4.06 <i>ft</i> aft of store nose
Forward ejector force	2400 <i>lb</i>
Ejector store length	0.33 <i>ft</i>
Roll moment of inertia, I_{xx}	20 <i>slug - ft²</i>
Pitch moment of inertia, I_{yy}	360 <i>slug - ft²</i>
Yaw moment of inertia, I_{zz}	360 <i>slug - ft²</i>
Freestream Mach number	0.95
Aircraft angle of attack	0.0 <i>deg.</i>
Pressure Altitude	26000 <i>ft</i>

system for the store is defined. The c.g. location of the store is chosen for the origin of this axis system. Mass and moment of inertia values for the store is given next. The forces acting on the store which are used for the trajectory calculations are selected in the same menu. For the present calculations, aerodynamic, gravitational and point forces are taken into account.

Aerodynamic force input requires the zone numbers of the store domain. The zones of the sting are not used in the aerodynamic force calculations. Therefore, multi-block grid generation is required for moving body problems if any section of the body is not used for the aerodynamic force calculations.

Point forces are used for the ejector force modelling. Any number of point forces can be added to the simulation. Frame of reference is chosen as the inertial axis for the ejector force applications. Point of application of the ejector force is defined in the inertial coordinate axis system. Ejector force applied can be a function of time or any of the three axis and three rotations. In this study, ejector forces are taken as constant and applied on the store until the store displaces 0.1 meters in downward direction in the inertial axis coordinate system.

Finally, using the Set-up Grid Motions menu, the zones that will move with the body coordinate axis system is chosen. The zones of the store and the sting are chosen together at this time. The parameters related to the validation test case are summarized and given in Table 4.3.

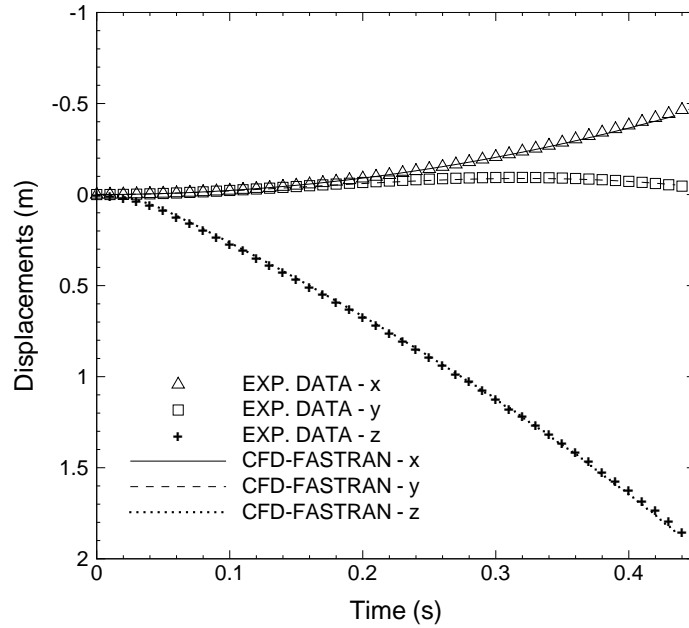


Figure 4.22: Comparison of linear displacements of the store with the experimental data[8], wing-pylon-store validation case, $M=0.95$

4.4.4 Separation Results of the Wing-Pylon-Store Test Case

Wing-pylon-finned store test case [8] is solved using the *CFD-FASTRAN* Euler solver code with overlapping grid methodology. The results given in this section represent the linear and angular displacements as well as the velocities and pressure distributions on the store at four different angular positions and the time histories of the force coefficients. It is observed that all of the major trends are captured when one compares the results with those given in [21].

4.4.4.1 Linear and Angular Displacements of the Store

Linear displacements graph are drawn with respect to the store's center of gravity location at the carriage position and given in Figure 4.22. Store moves backward and downward with the effect of gravity and the ejector forces after its release. Movement towards wing inboard side changes direction after $t = 0.32$ seconds. At this real time, the store is almost 1.3 meters away from the pylon. Actually, the side force acting on the store towards the wing inboard side starts decreasing linearly after separation and changes sign at $t = 0.16$ seconds. All displacements in three directions are in very good agreement with the experimental data [8].

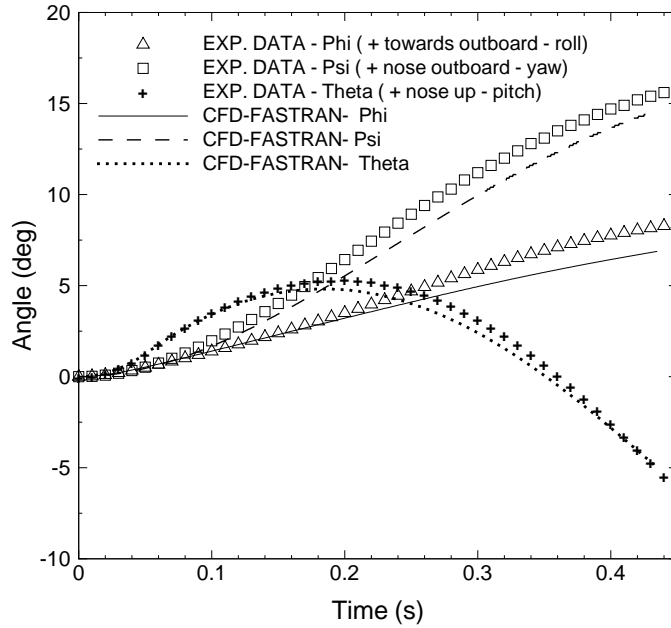


Figure 4.23: Comparison of angular displacements of the store with the experimental data[8], wing-pylon-store validation case, $M=0.95$

Angular displacements graph are drawn with respect to the coordinate system originated at the store's center of gravity location and given in Figure 4.23. Total forces acting on the store result in a pitch up, yaw and roll to the outboard motion after its release. Pitch up motion is mainly due to the ejector forces acting on the store for a real time of $t = 0.06$ seconds.

After the effect of the ejector forces vanishes, aerodynamic forces acting on the store take the control and result in a pitch down moment on the store. Store starts pitching down movement after time $t = 0.2$ seconds. The maximum pitch up angle calculated by Euler is 4.9 degrees whereas experimental data shows a maximum of 5.3 degrees. Discrepancy from data starts at time $t = 0.134$ seconds but the trend of the curve is almost the same with the experimental data. The maximum angular difference is 0.74 degrees, which occurs at $t = 0.24$ seconds.

Store rolls towards the outboard side of the wing after its release. The trend of the curve is almost the same with a shift in values from the experimental data. The discrepancy from the experimental data starts at time $t = 0.06$ s, almost at the end of the ejection. Maximum discrepancy from the data is 1.24 degrees at time $t = 0.3$ seconds.

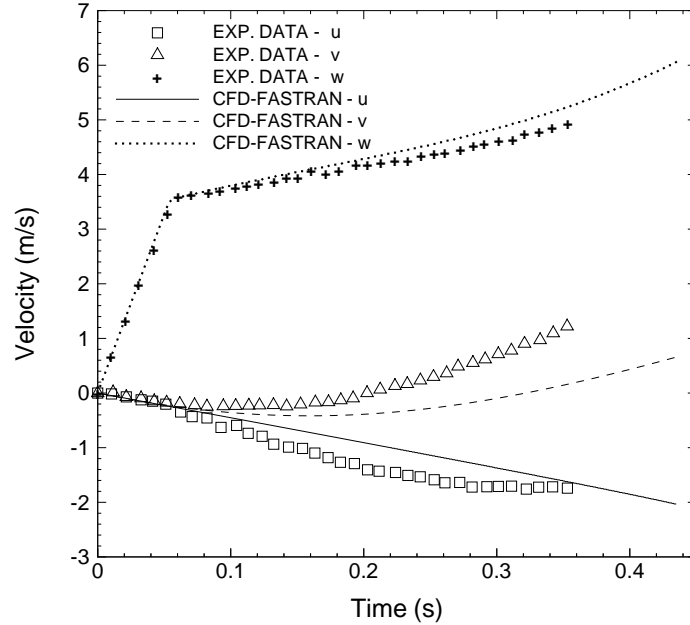


Figure 4.24: Comparison of linear velocities of the store with the experimental data[21], wing-pylon-store validation case, $M=0.95$

Yawing moment acting on the store is towards to the outboard of the wing. The trend of the curve is again the same with the experimental data. The discrepancy from the data starts at $t = 0.17$ seconds, and the difference increases till the end of the calculations. The maximum difference between the present calculations and the available data is 1.34 degrees.

4.4.4.2 Linear and Angular Velocities of the Store

Linear velocities of the store along its trajectory are given in Figure 4.24. Store moves down with an almost constant acceleration of 62.21 m/s^2 under the effect of ejector forces and its weight until $t = 0.06 \text{ s}$. After ejector forces disappear, linear velocity in downward direction increases with a lower acceleration. There is maximum discrepancy of 0.307 m/s between the data and the calculations.

Side velocity does not show a good agreement with the experimental data. In the experimental data, store has a negative side velocity of v after its release until time $t = 0.2$ seconds. However, present calculations have a time lag of 0.12 seconds for the side velocity to change its sign from negative to positive. At time $t = 0.32$ seconds, the difference between the side velocity calculations and the experimental data becomes 1.04 m/s .

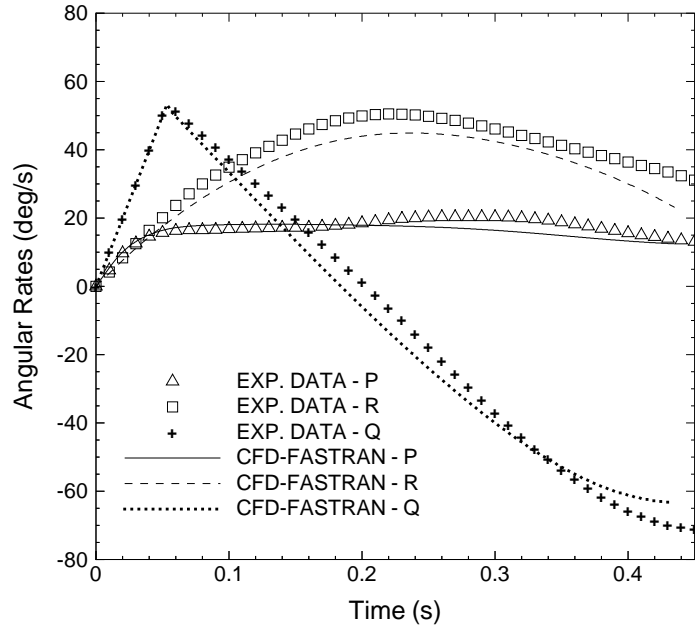


Figure 4.25: Comparison of angular velocities of the store with the experimental data[8], wing-pylon-store validation case, $M=0.95$

Backward velocity is linearly increasing in the negative x direction. There is discrepancy from the test data, but the trend is almost the same.

Angular rates are given in Figure 4.25. The results are in better agreement with the experimental data than linear velocities are. The angular pitch rate starts to decrease after $t = 0.06 s$, corresponding to the end of the stroke. The discrepancy between the angular yaw rate and the available experimental data can be seen after $t = 0.06 s$, but the trend of the curves are very similar. The angular roll rate has also similar trend with the experimental data. Differences between the values starts at $t = 0.2$ seconds after separation.

4.4.4.3 Forces Acting on the Store

The displacements are calculated from the forces and moments acting on the store. The order of the hierarchy is Forces, Velocities, Displacements. Therefore, calculation of the forces and moments are very important in finding the correct displacements.

Figure 4.26 shows the time histories of the non-dimensional force coefficients. Side force coefficient, CF_y , linearly increases from negative to positive values. This behavior results in the lateral displacement of the store as shown in Figure

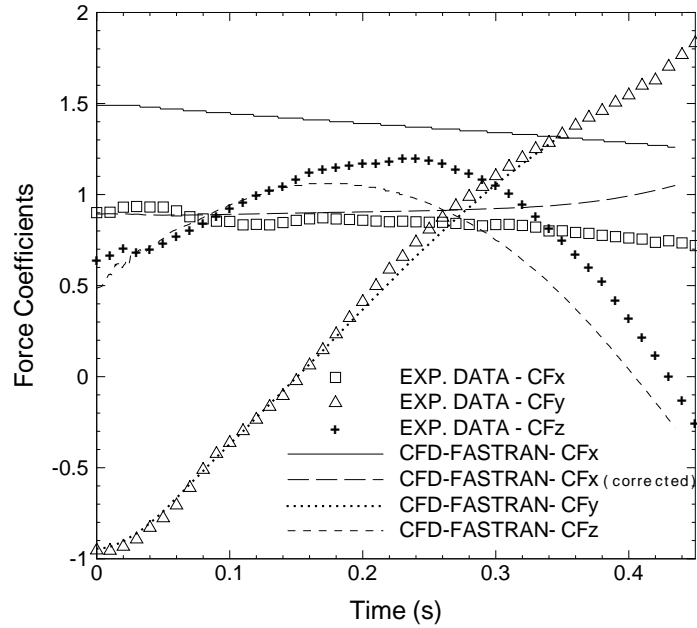


Figure 4.26: Comparison of force coefficients of the store with the experimental data[8], wing-pylon-store validation case, $M=0.95$

4.22. The discrepancy between the CF_y values and the data starts at time $t = 0.15$ ss.

The maximum difference between the calculated CF_y value and the data is 0.185. Store initially makes a pitch up motion due to ejector forces and has a positive angle of attack until $t = 0.2$ seconds. Therefore, non-dimensional force coefficient in z direction, CF_z , has a positive maximum value of 1.06 due to, then starts decreasing to negative values. The discrepancy from the data starts at time $t = 0.13$ seconds. But the trends of the curves are very similar.

There are two different CF_x curves are drawn. One of them is said to be corrected. This correction force is applied to the store and made for the base pressure. The direction of this force is always perpendicular to the base. The displacements are obtained with the base pressure correction applied to the store. Otherwise, the drag on the store would be higher than the experimental values causing much larger backward displacement.

The need for this base pressure correction is to compensate the pressure force in axial direction acting on the base which is not calculated due to the sting. In the experiments, this correction is also made for the trajectory calculations.

Generally speaking, no doubt that error is introduced to the results since the solution is obtained without the effects of viscosity. Ejector force approximation could also affect the Euler angles and rates since the correct ejector force modeling used in the experiment is not known exactly. Also the time accurate modeling of the flow would result in a different flowfield calculation than the quasisteady modeling of the experimental results. The effect of the sting mounted behind the store is investigated in the following section.

4.4.4.4 Separation Results Without Sting

The store geometry is modeled without the sting and the base of the store is smooth ended. The separation of the store is repeated at Mach 0.95. The results are compared with the store modeled with sting results, given in the previous sections.

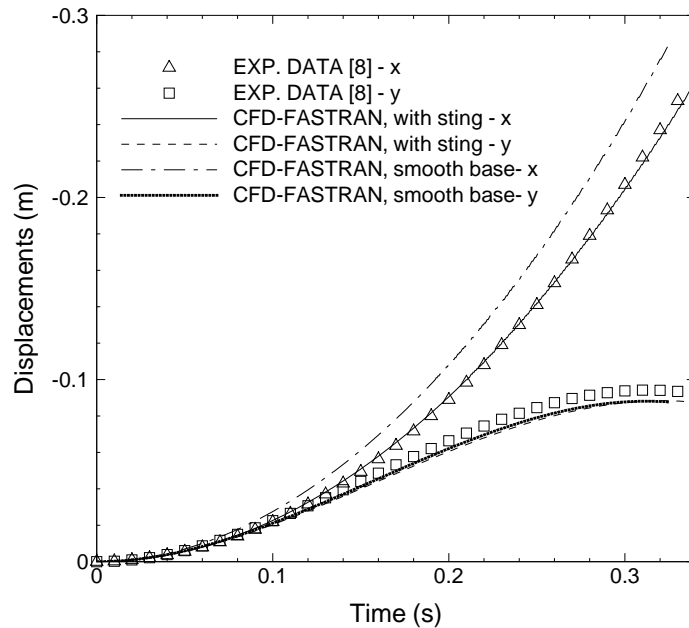


Figure 4.27: Sting effect on the linear displacements of the store, wing-pylon-store validation case, $M=0.95$

Linear displacements graphs are given in Figure 4.27. Z displacements for the two cases are calculated as the same. Therefore this graph is not included for the comparison. It is seen that y -displacements of the store is slightly improved when the sting is not used. However, major difference is observed in the x -

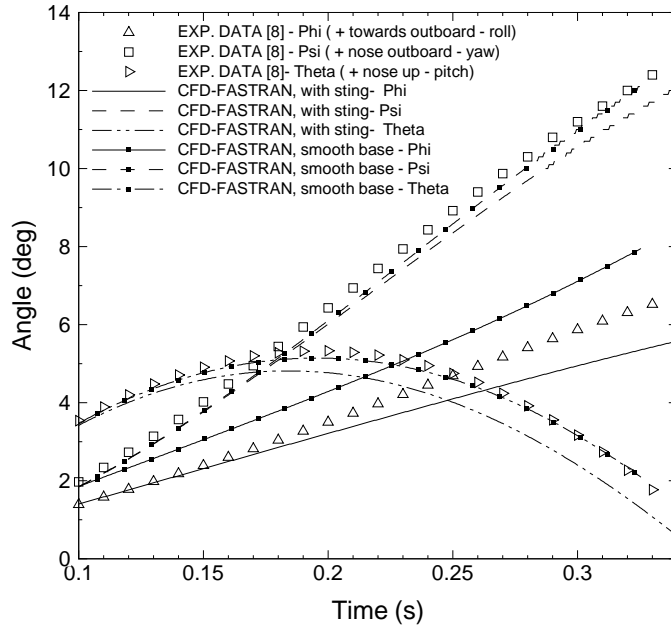


Figure 4.28: Sting effect on the angular displacements of the store, wing-pylon-store validation case, $M=0.95$

displacements. The axial force calculated is higher than the experimental data (Figure 4.30). This difference is due to that there is no base force correction applied when the sting is unmounted from the store. As a result, Euler solution has calculated a higher drag value than the experimental data.

Angular displacements graphs are given Figure 4.28. The differences between the two store models start after time $t = 0.1$ seconds. The first improvement observed is in the theta angle displacements. The theta angle (pitch) change in time are almost the same with the experimental data using the smooth based store model. Also, a better result is obtained for the psi angle (yaw) displacements. The phi angle (roll) displacements are calculated as higher than the available data, whereas it was lower for the solutions with the sting.

Linear velocities which are obtained using the smooth based store are almost the same with the previous results obtained using the store with sting, which are given in Figure 4.24. Angular velocities graph is given in Figure 4.29.

Roll angular rate, P , is calculated as much larger values from the experimental data. This increase in the roll rate results in higher roll angle values as seen in Figure 4.28. Pitch (Q) and yaw (R) angular rates are in better agreement with the

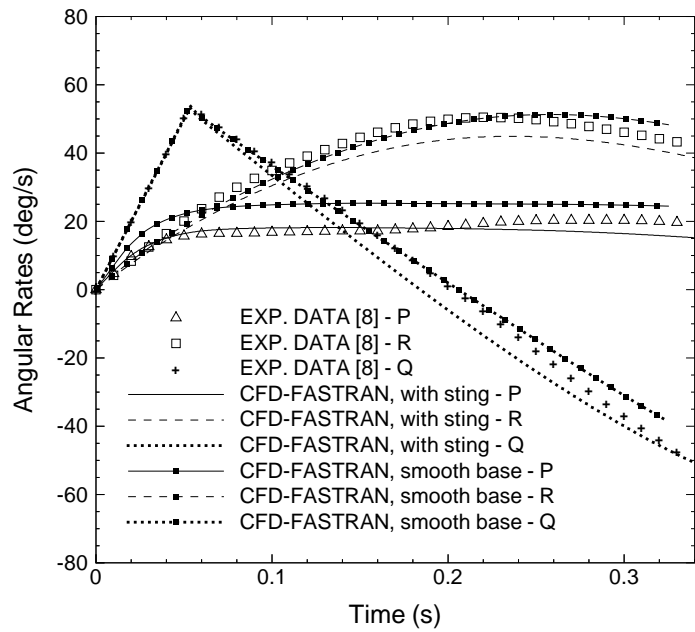


Figure 4.29: Sting effect on angular velocities of the store, wing-pylon-store validation case, $M=0.95$

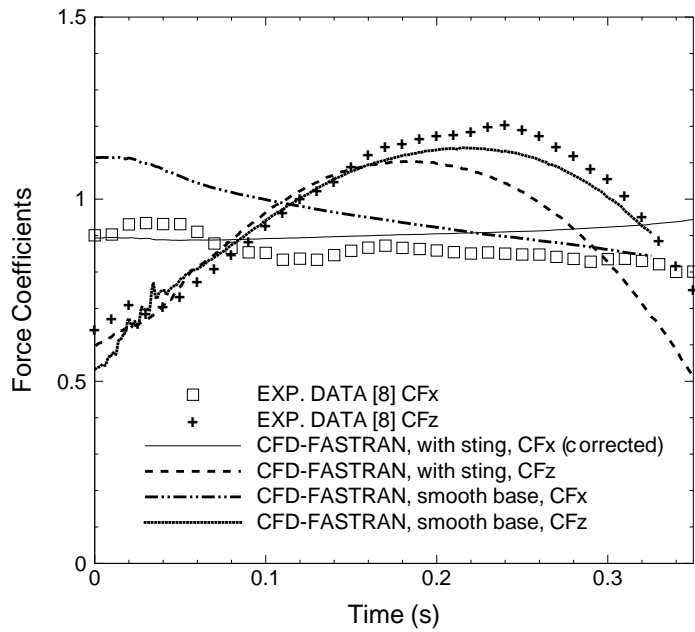


Figure 4.30: Sting effect on force coefficients acting on the store, wing-pylon-store validation case, $M=0.95$

experimental data than the store with sting model until $t = 0.25$ seconds. Later this time point forward, the results start to deviate from the experimental data.

The time history of force coefficients acting on the store graph is given Figure 4.30. Side force values are calculated the same for both store models, therefore this graph is not drawn for the comparison. The effect of base correction can be seen in CFx value graphs. It is observed that the CFx values of the smooth based store are in better agreement after time $t = 0.21$ seconds. This shows that as the store falls down, as a result of the weaker interaction between the store and the wing, better force values can be calculated on the store. The CFz values of smooth based model are again in better agreement with the available data compared to the model with the sting. However, this improvement in the results does not effect the linear z displacement of the store. This is due that the store is more driven by the inertial forces.

CHAPTER 5

RESULTS AND DISCUSSION

5.1 Overview

This chapter presents the results of two different store separation cases studied. The first case is the separation of a finned store from a wing-pylon configuration at Mach numbers of 0.3 and 0.6. The second case is the separation of a fuel tank from an F-16 aircraft wing alone and the full aircraft configurations. The first case is solved with both the Euler using the chimera methodology and the unsteady panel codes. The second case is solved only using the unsteady panel code. The aim is to compare the two methods of prediction tools and to find out which aspects of the store separation phenomenon could be captured with these two different prediction tools. The results are given in terms of time wise variations of the linear and angular displacements of the store along its trajectory after being released, the pressure distribution on the store in its captive position ($t = 0$ s) right before its separation and the time histories of the force coefficients acting on the store along its trajectory.

5.2 Configurations

Two different configurations are used in the present solutions. The first configuration is the generic wing-pylon-store configuration. The sting which was used in the validation studies is not modeled this time. Instead, the base of the store

is cut at the junction location of the store with the sting.

Second configuration is an F-16 aircraft configuration. Two different subcases are considered here using the same geometry; F-16 aircraft's wing alone-pylon-fueltank and a full F-16 aircraft configuration with the fueltank. These cases are used to investigate the effect of the fuselage on fueltank trajectory after its separation.

5.2.1 Wing-Pylon-Store Configuration

This configuration is the same as used in the validation studies except the sting is not mounted behind the store. The dimensions of the wing, pylon and the store are the same as given in Figures 4.9, 4.10 and 4.11. The store base is cut right at the junction location of the sting with the store as it is seen in Figure 5.1(left). There are two reasons for this modification. First, the panel code does not have the capability of selecting wall surfaces of a moving body frame individually for the force and moment values used in the trajectory calculation. Instead, the code includes all the forces and moments on the wall boundaries to the trajectory calculation which are moving with the store frame. Therefore, if the sting is used in the solution configuration, forces and moments acting on it will also be included in the trajectory calculations, which would yield to wrong values. The second reason is related to the wake modelling in the panel code. If the base of the store is smooth ended as it is given in Figure 5.1 (right), there would be no wake released from the store base. Therefore the modelling for the panel code will not be correct, since the discontinuity behind the store could not be modelled without any wake.

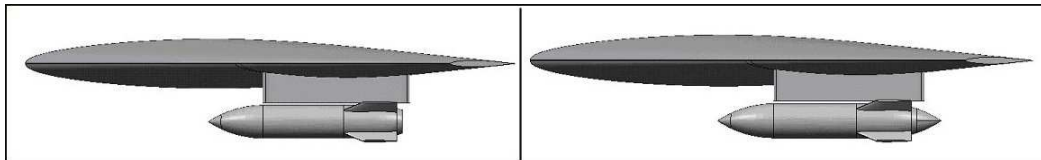


Figure 5.1: Side view of wing-pylon-store configuration, sharp cut-base (left) and smooth-base (right)

5.2.1.1 Grids and Paneling

The grid topology of the wing-pylon-store configuration for the Euler solution is the same as used in the validation test case. Topology is suitable for Chimera technique. The difference in two solution domains is due to the sting only. Detailed description of the grid topology can be found in Section 4.4.2.

The surface paneling for *USAERO* code is also created using the *CFD-GEOM* software. The surface panels are then exported to a compatible format for *USAERO* using a FORTRAN code [34]. The surface panel warp and surface normal directions are checked and corrected with *SPIN(g)*, the pre-processor of *USAERO*. Other modifications such as ordering, splitting, and joining of panel groups (patches) are also performed using the *SPIN(g)*. For free shear layer simulation, a wake model is also introduced using the other pre-processor, *SPIN(w)* of *USAERO*. The detailed explanations for modeling in *USAERO* can be found in Ref. [34, 35].

2712 body panels are used to model the wing-pylon-store configuration. Wake modeling is used for the wing, pylon, store fins and the store base. Paneling and wake modeling of this configuration is given in Figure 5.2.

5.2.1.2 Computations

Steady-state and implicit Euler solutions are obtained before the time accurate computations are started. Roe's approximate Riemann solver scheme is used for flux computations, which is first order spatially accurate. Second order accuracy is obtained using Minmod ($1/r$) limiter. CFL number is increased from 1 to 20 in 200 iterations for steady-state calculations. Time step is taken as 0.00005 for the transient computations. CPU computation time for 1 time step takes an average value of 156 s using a P4 2 GHz stand-alone computer. 5700 time step solutions take maximum of 1.9×10^5 CPU time using a parallel computing cluster built up with 16 PIII 733 MHz CPUs. The domain decomposition in structured grids for parallel computations is performed by assigning of blocks to different CPUs. Therefore, the blocks must be created nearly of the same size in order to obtain a well balanced, equal load distribution.

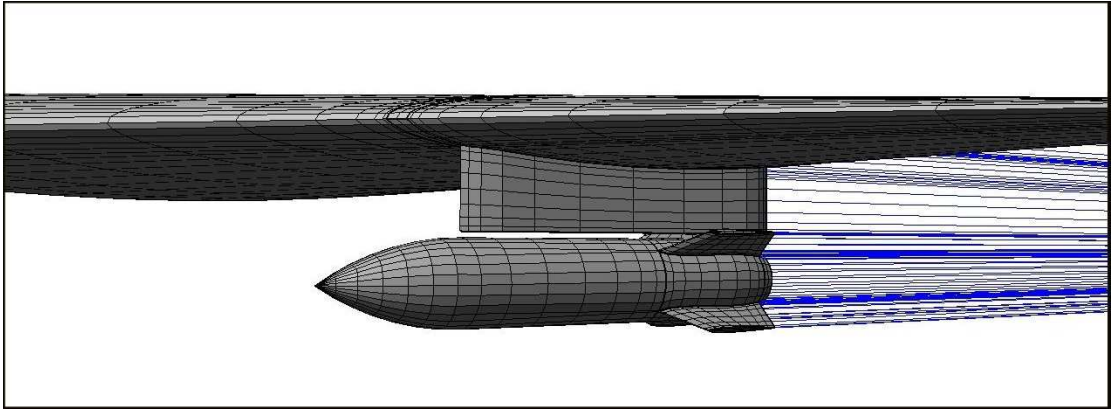


Figure 5.2: Paneling and wake modeling of wing-pylon-store configuration for USAERO

For the unsteady panel code solutions a time step of 0.001 is used. 30 time steps are used in order to establish the wake before the separation process starts. Boundary layers are taken into account by activating the integral boundary layer method coupling with potential flow solution. A direct matrix solver, LAPACK, is used for the matrix inversions. Solutions are obtained using a SGI-Octane stand-alone computer. The average CPU time needed for a time step of solution using 2712 surface panels including wake panels is around 106 seconds. The first time step takes a CPU time (without wakes) of 22.67 seconds and the last time step takes 208.80 seconds. F-16 aircraft configuration with 6046 body panels takes about 20 hours of CPU time for 0.32 seconds of real time duration of transient solution.

5.2.1.3 Smooth base-Sharp Cut base Force Comparisons

In Euler solution, calculated drag values include the pressure forces, but excludes the viscous effects. Due to inviscid nature of the flow, base drag value could not be calculated correctly. The panel code gives drag value after the boundary layer coupling, therefore the total drag predicted by the panel/boundary layer method includes the skin friction drag as well.

Base wake model is used in USAERO for the flow separation at the base-cut section. In order to investigate the effect of base cut and the separated flow,

a series of test cases are run with both codes using the configurations given in Figure 5.1. Mach number is taken as 0.3. The store base is smoothed in order to have a reasonably attached base flow. Base wake model is not used for this case in USAERO solution. The comparison of the resultant force and moment coefficients with the base-cut model are given in Tables 5.1 and 5.2, respectively.

The drag values which are calculated for smooth base configurations are very close to each other. It is observed that smoothing the base of the store reduces the drag value as obtained by the Euler code. The reverse effect is observed when the panel code is used. Drag value is reduced when the base wake model is introduced to the solution. The normal force coefficient CF_z is found to be the same using both methods for the base-cut configuration. Side force value is found to be half of the panel code when the Euler code is used.

Table 5.1: Force coefficients on the store in its captive position, smooth and sharp-cut base comparisons, $M=0.3$

Smooth base	CF_x	CF_y	CF_z	Sharp cut base	CF_x	CF_y	CF_z
FASTRAN	0.214	-0.444	0.511	FASTRAN	0.384	-0.449	0.695
USAERO	0.196	-0.227	0.668	USAERO	0.128	-0.285	0.695

Table 5.2: Moment coefficients on the store wrt. c.g. location in its captive position, smooth and sharp-cut base comparisons, $M=0.3$

Smooth base	CM_x	CM_y	CM_z	Sharp cut base	CM_x	CM_y	CM_z
FASTRAN	0.0945	1.2307	0.1153	FASTRAN	0.0967	1.702	0.1261
USAERO	0.0101	1.3082	0.2099	USAERO	0.0110	1.465	0.0225

5.2.2 F-16 Aircraft Configurations

F-16 Fighting Falcon is a multi-role fighter aircraft in TUAf. This aircraft was previously analyzed by [35, 36] using CFD tools. In Ref [35], aerodynamic analysis of external store carriage on the same aircraft was investigated using the panel code, *VSAERO*. It is a low order panel code, which is the steady version of the unsteady panel code *USAERO*. In the other Ref [36], loads on different stores are calculated at the carriage position using the same Euler code *CFD-FASTRAN*. In this study, solutions were obtained using the unstructured grids. Both of these previous studies were concentrated on the effect of the stores on the aircraft

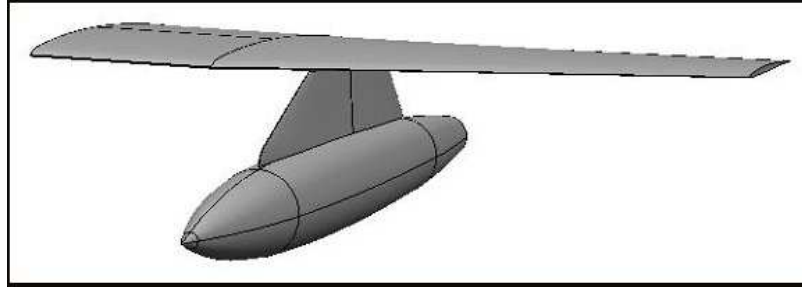


Figure 5.3: F-16 Wing-Pylon-Store configuration

stability characteristics and the drag increase due to store carriage.

In this study, two configurations of the F-16 aircraft are considered. First one is the F-16's wing alone-pylon-store configuration as shown in Figure 5.3. Root section of the wing is extruded until the symmetry plane of the aircraft in order to diminish the strong compressed flow region between the symmetry boundary and the store. In its captive position, fuel tank has a negative angle of attack of 3° due to its installation. The mass of the fuel tank is taken as 250 kg as if it is nearly empty before the separation. Moment of inertia calculation is done by the code *USAERO* itself, by assuming that the given mass value is evenly distributed over the entire store. The c.g. location of the fuel tank is chosen at the mid point location of the longitudinal axis passing from the nose of the store. The ejector forces applied to the store are placed at 15cm. aft and forward of the c.g. location, with values of 4000N and 6000N respectively.

The second one is the full F-16 aircraft configuration as shown in Figure 5.4. Both cases have a pylon under the wing, and a fuel tank of 370 gallon capacity is used as the store. The trajectories of the fuel tank after it is separated from these two configurations are compared. The effect of fuselage on the separation phenomenon is therefore investigated.

Surface panelling of both configurations are created using the *CFD-GEOM*. 6046 surface panels are used for the paneling of the symmetric half of the F-16 aircraft. Same procedure is used for the wing-pylon-store configuration for panel warp and surface normal controls.

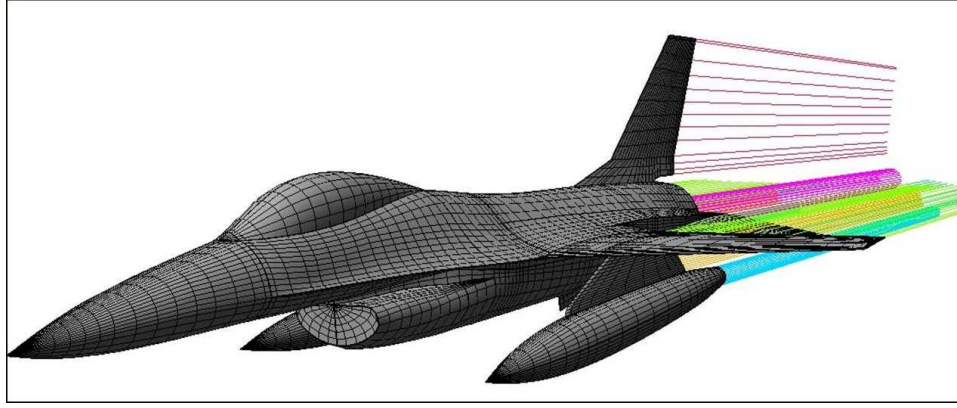


Figure 5.4: F-16 aircraft full configuration paneling and wake modeling

5.3 Results

This section includes the results and discusses the separation process for both cases.

First, separation of the store released from a generic wing-pylon configuration is solved using the Euler and the unsteady panel code. Linear and angular positions of the store along its trajectory and non-dimensional pressure coefficient distribution on the store at its captive carriage position are calculated for two different Mach numbers of 0.3 and 0.6. The solutions obtained are compared for the two solutions. Differences between the two methods of solution are further discussed.

Secondly, the separation of a fuel tank from an F-16 aircraft wing-pylon and full aircraft configurations are considered for two different Mach numbers of 0.3 and 0.6. The effect of the fuselage on the fuel tank along its trajectory is investigated by comparing the results obtained. Linear and angular positions of the store along its trajectory and the non-dimensional pressure coefficient distribution on the store its carriage position are used for the comparisons of the differences between the two configurations.

5.3.1 Wing-Pylon-Store Separation Results

This study is performed to investigate in what respects the Euler and the unsteady panel codes resemble and differ from each other in the calculation of the trajectories. Solutions are performed at two Mach numbers of 0.3 and 0.6 in

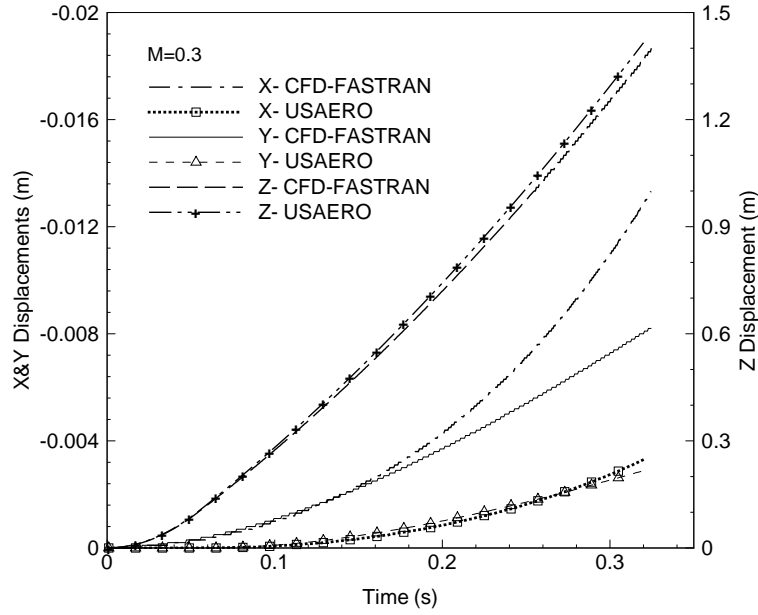


Figure 5.5: Linear displacements of the store after separation, comparison of CFD-FASTRAN and USAERO solutions at $M=0.3$

order to discover the effect of Mach number on the results obtained by the two methods. The duration of the separation is 0.32 seconds of real time. At first, the capability of the Euler solver at Mach 0.95 is investigated and the results obtained are compared with the experimental data [Section 4.4]. Unfortunately, there are no experimental results available for the later Mach number studies. The results are given and discussed for the linear and angular displacements of the store, non-dimensional pressure coefficient distribution and the time histories of the force coefficients acting on the store.

The linear displacements of the store during the separation process for Mach 0.3 are given in Figure 5.5. The X and Y displacements are very small compared to Z displacement. Therefore, a different scale has to be used for Z displacement graphs. The differences in the captive carriage forces are reflected in the X and Y displacements. Although the same trends are captured by both codes, significant discrepancies are observed in the X and Y components. Z displacements give almost the same at this Mach number. It is observed that the CF_z values calculated with both codes are nearly the same at Mach 0.3.

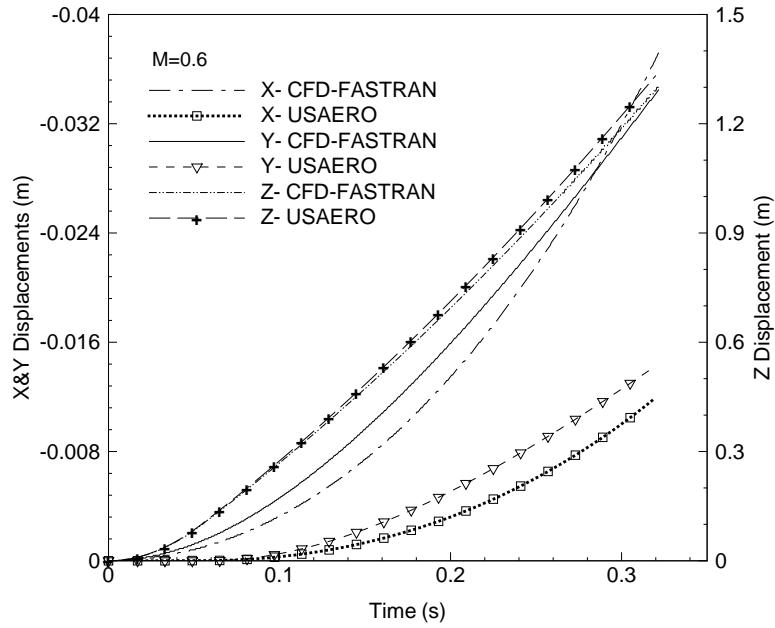


Figure 5.6: Linear displacements of the store after separation, comparison of CFD-FASTRAN and USAERO solutions at $M=0.6$

The linear displacements of the store during separation process for Mach 0.6 are given in Figure 5.6. The X and Y displacements are four times larger than the values for Mach 0.3 results, but still they are very small when compared with the Z displacement. Z displacements are very close to each other as it was for Mach 0.3 case.

Angular orientations can be seen in Figures 5.7 and 5.8 for Mach 0.3 and 0.6, respectively. Yaw and roll angles are small when compared with the pitch angle. Therefore, a different scale had to be used for pitch angle displacement. Yaw and roll angles have the same trends for both Mach numbers. However, pitch angle variations for Euler solutions has different trends for the two Mach numbers. Store pitch angle continuously increases at low Mach number. For Mach 0.6, pitch angle change rate decreases at the end of the simulation. This attitude of the store is similar to the Mach 0.95 solution. The pitching moment due to aerodynamic forces starts to take the control after the ejection forces disappear.

The largest discrepancy is observed in the roll angle predictions by both of the codes at the given Mach numbers, whereas the predictions for the yaw angles by both of the codes are in better agreement. This agreement is getting better with increasing Mach number.

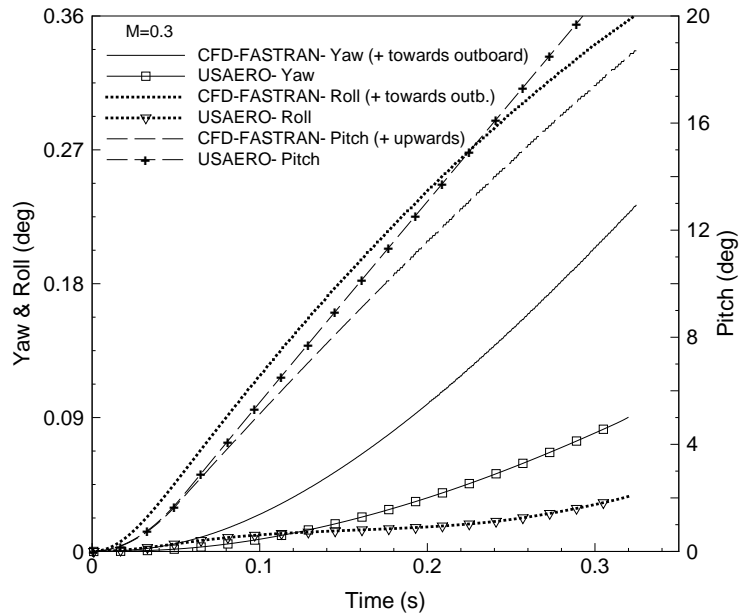


Figure 5.7: Angular displacements of the store with respect to its body axis after separation, comparison of CFD-FASTRAN and USAERO solutions at Mach 0.3

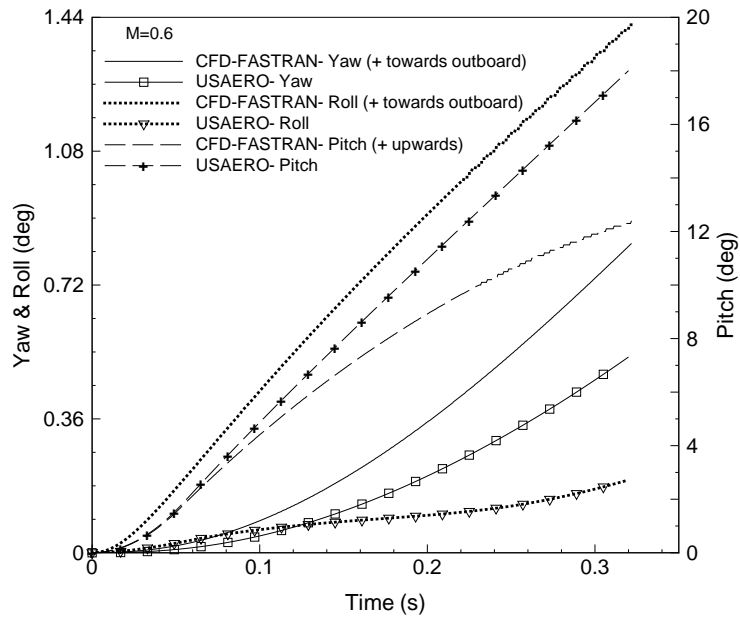


Figure 5.8: Angular displacements of the store with respect to its body axis after separation, comparison of CFD-FASTRAN and USAERO solutions at Mach 0.6

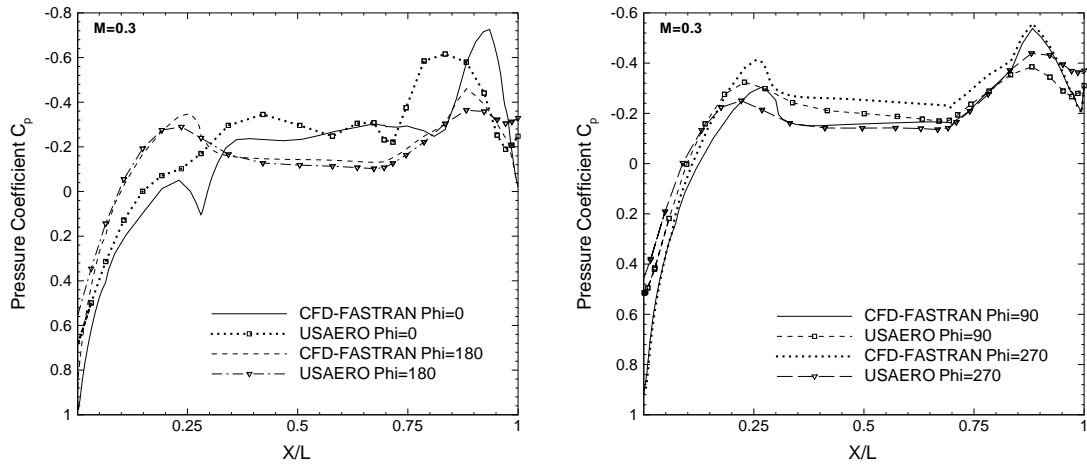


Figure 5.9: Pressure distribution on the store in its captive position, comparison of USAERO and CFD-FASTRAN solutions at $M=0.3$

Pressure distributions on the store in its captive position are drawn at $\Phi = 0^\circ, 90^\circ, 180^\circ$ and 270° angle planes and are given in Figures 5.9 and 5.10. The pressure distributions calculated with both codes have the same trend. Interaction between the pylon and the store can be observed in the Euler solution at $\Phi = 0^\circ$ angular cut. The same compression is also observed in the panel method but with much strength.

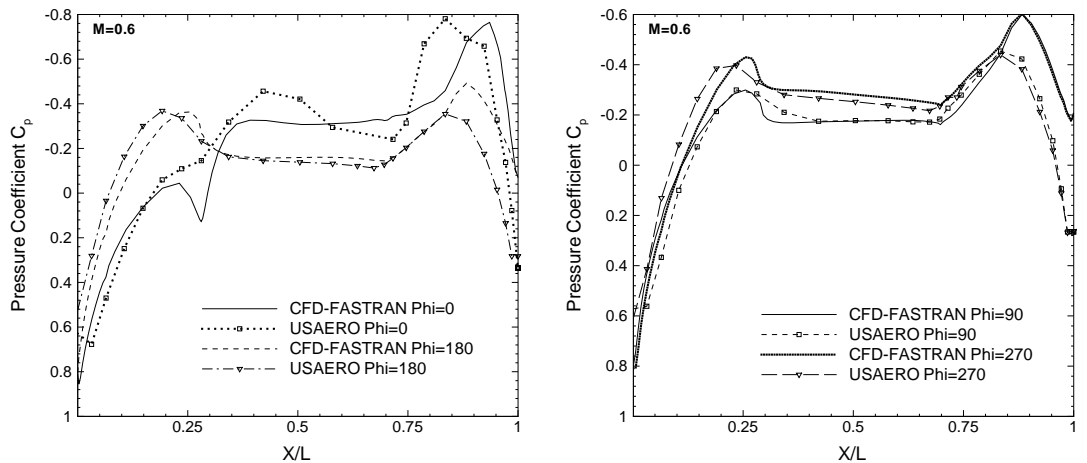


Figure 5.10: Pressure distribution on the store in its captive position, comparison of USAERO and CFD-FASTRAN solutions at $M=0.6$

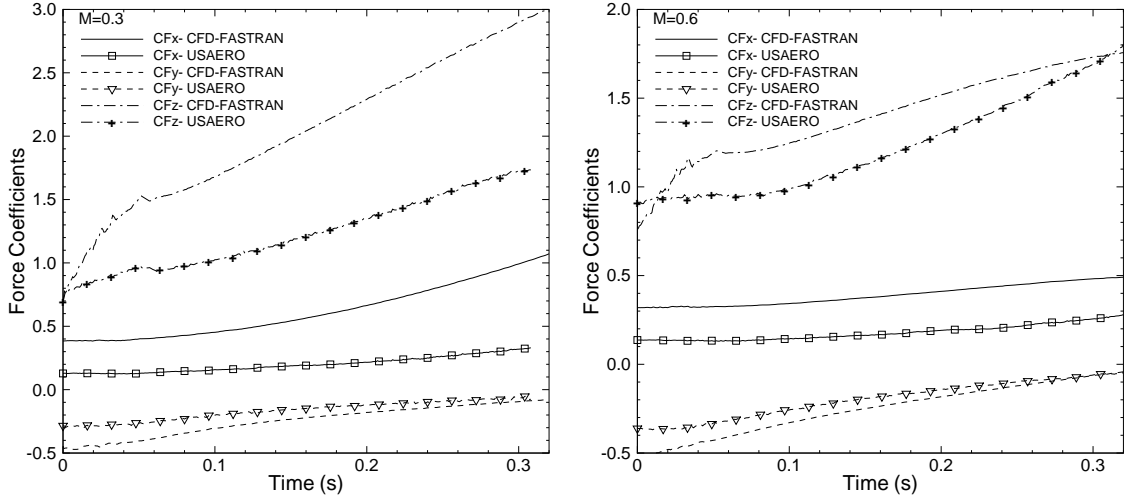


Figure 5.11: Time Histories of force coefficients acting on the store along its trajectory, comparison of USAERO and CFD-FASTRAN solutions at $M=0.3$, $M=0.6$

For $\Phi = 90^\circ$, 180° and 270° angles, *CFD-FASTRAN* calculates lower C_p values than the panel code after $X/L = 0.75$. Same behavior is observed when the C_p distributions are compared with the experimental results in the wing-pylon-store case at $M=0.95$. This difference can be attributed to the nature of the Euler solver which excludes the effects of viscosity. Boundary layer coupling option when introduced to the panel method improves the C_p distributions obtained by the *USAERO* code. This difference in pressure distribution results in lower force and moment coefficients values than obtained in *CFD-FASTRAN*.

Time histories of force coefficients are given in Figure 5.11 for $M=0.3$ and $M=0.6$. The trends are in better agreement at $M=0.6$ than $M=0.3$ results. In particular, CF_z and CF_y values become very close to each other at $t=0.32$ seconds, where the store is more than 1 meter away from the wing. Also the pitch angle is almost 13° for Euler and 17° for the panel code at that location. It is well known that the predictions by both the Euler and the panel codes are not very reliable at high angles of attack. This may be a result to see that both codes have the same error in that case. A summary of the force and moment coefficients at captive carriage state are given in Table 5.3.

Since there are no experimental results available for these configurations, the

Table 5.3: Summary of the force and moment coefficients acting on the store in its captive carriage position, comparison of USAERO and CFD-FASTRAN solutions at M=0.3

Mach 0.3	CF _x	CF _y	CF _z	CM _x	CM _y	CM _z
FASTRAN	0.384	-0.449	0.695	0.0967	1.702	0.1261
USAERO	0.128	-0.285	0.695	0.0110	1.465	0.0225

Table 5.4: Summary of the force and moment coefficients acting on the store in its captive carriage position, comparison of USAERO and CFD-FASTRAN solutions at M=0.6

Mach 0.6	CF _x	CF _y	CF _z	CM _x	CM _y	CM _z
FASTRAN	0.319	-0.507	0.758	0.0938	1.839	0.1111
USAERO	0.137	-0.362	0.912	0.0130	1.882	0.0406

discussions are based on the comparisons of the results of the panel code with the Euler code. More could be said after comparing the computational results with those of the wind-tunnel test results

5.3.2 Fueltank Separation Results from F-16 Aircraft

This study is performed to find the trajectory of a fueltank separated from an F-16 aircraft and to investigate the effect of the fuselage on the store separation. Solutions are performed at a Mach number of 0.3 using the *USAERO* panel code only. The duration of the separation analysis is 0.32 seconds of real time. Unfortunately, there are no experimental results available for this analysis. The results are given in linear and angular displacements of the store in its trajectory and the pressure distribution on the store in its captive position (t=0s) right before its separation from the aircraft and the time histories of the force coefficients acting on the fueltank along its trajectory.

Linear displacement graphs of the fueltank are given in Figure 5.12. Z displacements for both configurations are almost the same. X displacement for the wing alone configuration has the same trend with that of the full aircraft configuration, but the drag value is higher as it can be seen in Figure 5.15. Therefore, the store separated from the wing moves faster backwards when compared with the full aircraft configuration. The most important difference is observed in the Y displacement. The side force calculated on the store in the wing alone case is very

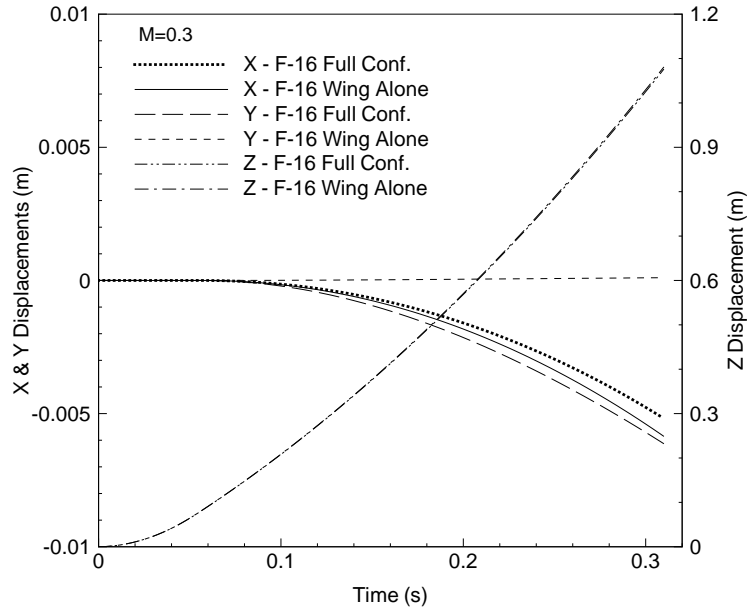


Figure 5.12: Linear displacements of the fuel tank after separation, $M=0.3$

small when compared with the force obtained for the full aircraft configuration. As a consequence of this side force, an inboard movement of the store is observed in the full aircraft configuration whereas the opposite is true for the wing alone case.

Angular displacement graphs of the fuel tank are given in Figure 5.13. Pitch angle has the same trend for both cases. However, yaw and roll angles have shown opposite behavior. The store separated from the full aircraft configuration rolls outboard and yaws to inboard whereas the store separated from the wing exhibits opposite angular motions.

Pressure distribution graphs are given in Figure 5.14. Compression due to the effect of the pylon is observed with both configurations at $\Phi = 0^\circ$ angular plane. Pressure distributions at $\Phi = 90^\circ$ and $\Phi = 270^\circ$ angular plane cuts are almost the same for wing alone configuration and it is observed that there is no significant movement of the store in that direction after separation. However, the pressure on the inboard side of the store is lower than that on the outboard side for the full aircraft configuration. Therefore, the store has a movement towards inboard of the wing when separated from the full aircraft configuration.

There is a significant difference in side forces as observed in Figure 5.15. The

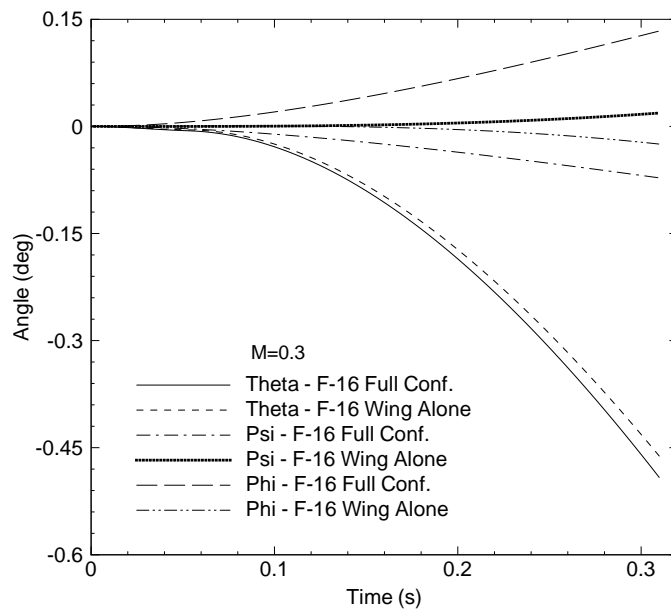


Figure 5.13: Angular displacements of the fuel tank after separation with respect to its body axis, $M=0.3$

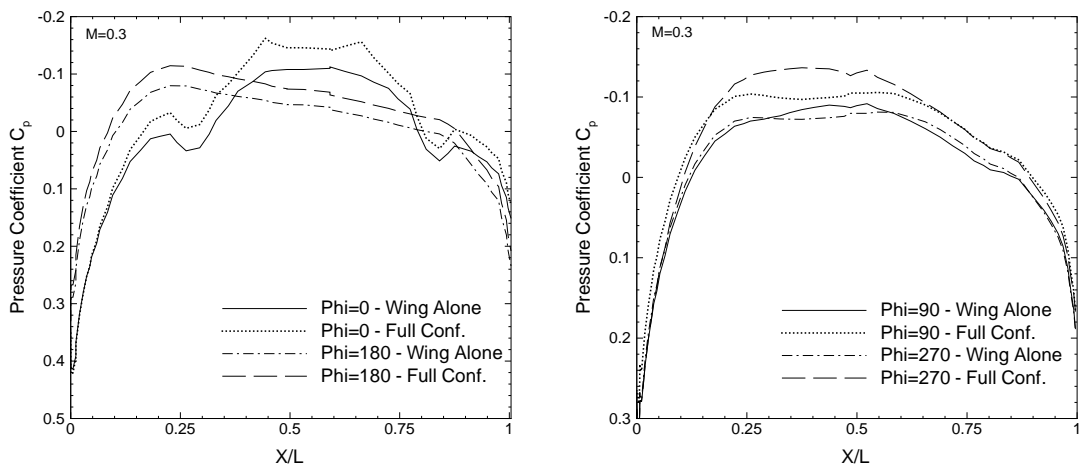


Figure 5.14: Pressure distributions on the fuel tank in captive position, $M=0.3$

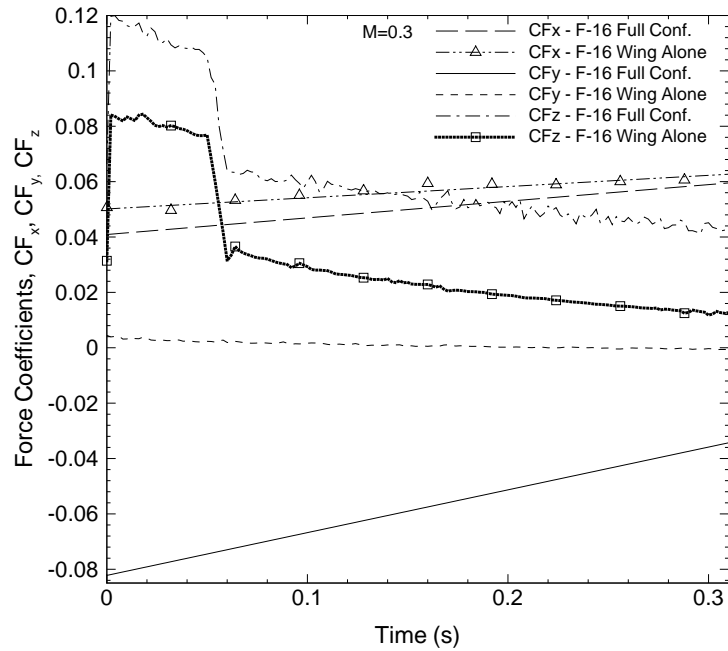


Figure 5.15: Time histories of force coefficients acting on the fuel tank along its trajectory, $M=0.3$

negative side force on the store when released from the full aircraft configuration shows a linear decrease as the store moves downwards. This result shows the predominant effect of including the fuselage to the modeling of a fuel tank separation problem. Also an increase in the lift and a decrease in the drag coefficient acting on the store are also observed. A summary of the force and moment coefficients at the captive carriage state are given in Table 5.5.

The results show that wing alone solutions for the fuel tank separation can not be substituted for full aircraft solutions. The displacements of the fuel tank will increase and become more important at higher Mach numbers.

Table 5.5: Summary of the force and moment coefficients acting on the fuel tank in its captive carriage position right before separation, $M=0.3$

Fuel tank	CFx	CFy	CFz	CMx	CMy	CMz
Wing Conf.	0.0506	0.0044	0.0314	0.0004	-0.7359	-0.0021
Full Conf.	0.0427	-0.0823	0.0664	0.0034	-0.7585	-0.0517

CHAPTER 6

CONCLUDING REMARKS

In this thesis, store separation from two different aircraft configurations are solved using commercially available CFD codes; CFD-FASTRAN an implicit Euler solver and an unsteady panel method solver USAERO, coupled with integral boundary layer solution procedure. Euler solutions are obtained using chimera methodology. The computational results are validated against the available experimental data of a generic wing-pylon-store configuration at Mach 0.95. Same configuration is used for the comparison of unsteady panel method with Euler solution at Mach 0.3 and 0.6. Trajectories of a fuel tank separated from an F-16 aircraft wing and full aircraft configurations are solved at Mach 0.3 using only the unsteady panel code the effect of the fuselage is observed on the trajectories and angular orientations of the fuel tank.

Preliminary studies are performed in order to test the capabilities of *CFD-FASTRAN* flow solver, the chimera algorithm and the 6DOF body motion module. The first case is the steady state solution of the store alone configuration and two stores side-by-side cases at Mach 0.95. The store grids and the background grid are created independently and chimera methodology is used in the solution process. The pressure coefficient distribution on the store is compared with the available experimental data. Both the pressure distribution on store alone and two stores side-by-side cases show a very good agreement with the experimental data. This shows that even there is an interaction between two bodies, the

chimera methodology works fine with the Euler solver.

The second case is the steady state Euler solution of the wing-store configuration. *CFD-FASTRAN* solution is compared with another Euler solver [33]. In order to eliminate the grid dependency, same grids are used in the solution using both codes. Mach number is taken as 0.95 and chimera methodology is used with both codes. Pressure distributions on the wing surface at two different spanwise locations and store surface at 4 axial cuts are compared with each other. All the pressure distribution trends are the same on both wing and the store. Shocks are found almost at the same locations with both codes. However, the Euler code [33] smoothes the C_p curves at the shock locations due to its dissipative terms and *CFD-FASTRAN* calculates the shock locations more accurately.

The third case is the store separation test case using the generic wing-pylon-finned store configuration. The linear and angular displacements and velocities of the store is compared with the available experimental results [8]. The time history of force coefficients and the pressure distribution on the store at four different angular cuts are also used for the comparison purposes. Preliminary study on the number of cells to be used for the interpolation between the store and the pylon show that the pressure distribution on the store is highly effected with this grid node number.

All major trends of the linear and angular displacements and velocities are captured using the chimera methodology. Store moves backward, downward and towards inboard after separation. There are some discrepancies from the experimental data. The main difference between the calculated force coefficients and the available data is seen at C_z value. However, all the trends in forces, velocities and displacements graphs support each other.

The error is introduced to the results since the effect of viscosity is neglected using the Euler equations. The ejector forces are not modeled correctly, since they are not recorded during the experiments. This approximation on these forces may affect the results. Also the experiment results are not time accurate since CTS technique was used in the experiments, which is a quasisteady method. The time accurate computations are performed during the solution process, therefore

error could be introduced to the results. Since the sting is mounted behind the store in the experiments, a correction base force is applied on the store in numeric computations. Otherwise, high drag values are obtained and this would yield wrong displacements in the axial direction. Despite all these errors, from the results obtained so far, the *CFD-FASTRAN* solver can be used in the store separation problems.

The possible effects of the sting on the trajectory characteristics are also investigated. For this purpose, the sting is unmounted from the store and the store base is smoothed as its nose shape. The calculations are repeated at Mach 0.95.

It is seen that the linear displacements are not affected except the axial displacement. The axial displacements are higher than the experimental data since the base of the store is not the same as used in the experiments. Also no base force correction is used for the solutions. Therefore, this result is as expected. Better trajectory results are obtained in pitching and yawing motions. Linear velocity curves are not affected much. However, higher roll rate values are calculated when the base of the store is smoothed. This results in higher roll angle displacements than the experimental data and the previous solution with the sting. Pitch and yaw angle rates are in better agreement with the experimental data until $t=0.25$ seconds. Side force coefficient histories for both configurations are the same. However, the force component in the z direction has better coherence with the experimental data. But this improvement on the force coefficient is not reflected to the z displacements. This shows that the store moves downward under the effect of the inertial forces. Axial force values of the store are in better agreement with the experimental data after 0.2 seconds. This is the result of weaker interaction between the store and the wing-pylon, which highly affects the axial force calculations.

Two different store separation cases are studied. The first case is the separation of a finned store from wing-pylon configuration. This configuration is solved both with the Euler and unsteady panel codes at Mach numbers of 0.3 and 0.6. The aim is to compare the two methods of prediction tools and to find out which

aspects of store separation phenomenon could be captured.

Due to the weight of the store and the ejector forces, X and Y displacements of the store are very small compared to the Z displacement of the store at both Mach numbers. Z displacements of the store are the same when calculated with both codes. But axial and lateral displacements found by using the Euler code are more than twice as large as the panel code solutions. However, depending on the separation criteria, these displacements can be neglected since they are very small.

Increase in Mach number increases the magnitudes of axial and lateral displacements but do not effect the downward displacement. This shows that the store is displaced under the effects of inertial forces. All the trends of the curves are the same.

Yaw and roll angles are small compared to pitch angle for both Mach numbers. Yaw and roll angles have the same trends using the both codes for both Mach numbers, but the pitch angle variations differs for Euler solution at Mach 0.6. The trend of the curve shows that aerodynamic forces start to take the control of the store trajectory at Mach 0.6.

The compression due to pylon at carriage position is observed with both codes but panel code calculates much in weaker strength. Boundary layer coupling option improves the pressure distribution obtained by the panel code. The trends of the pressure distributions are the same but the differences between the magnitudes starts after the fin location, where viscous effects are dominated.

Force coefficient histories of the store are in better agreement at high Mach number. Since no experimental results available, discussions are based on the comparison of the results of the panel code with the Euler code.

The second case is the separation of a fueltank from an F-16 aircraft wing-alone and full aircraft configurations at Mach number 0.3. The aim is to investigate the fuselage effect on the trajectory of the fueltank after separation. Solutions are obtained using the unsteady panel code.

The fuselage does not have any significant effect on the downward displacement of the fueltank in this configuration. Higher drag value is obtained in full

aircraft configuration than wing alone case, therefore the store moves faster towards the backward. The fuselage affects the side force exerted on the fuel tank, and fuel tank moves inboard after separation whereas the opposite is true for wing alone case. Also, the fuselage affects the roll and yaw motion of the fuel tank and these directions are reversed.

The modeling of a full aircraft configuration for the Euler solution using structured grids is a challenge. Instead of modelling the full aircraft configuration, one can model only the wing of the aircraft and perform the solutions. However, the results show that the wing is not a substitute for the fuselage. The compressed flow between the fuselage and the store highly affects the attitude of the store. This effect will be higher and becomes critical at high Mach numbers.

The same configuration can be modelled in less time and effort for a panel code than an Euler/Navier-Stokes solver. All the cases in the solution matrix using a panel code can be performed in a solution time needed for a unique Euler solution. However, solutions at high Mach numbers, which are close to transonic regimes must be obtained using a compressible Euler or Navier/Stokes solver.

Further research is also in progress for the store separation from wing-pylon-store configuration at Mach 1.2. The results will be validated with the available experimental data. Also, ACFD Challenge II configuration F-18/C with JDAM is obtained and will be modelled in CFD-GEOM using structured grids. The results will be compared with the available flight test data.

REFERENCES

- [1] Schindel, Leon H., *Store Separation*, AGARD-AG-202, 1975.
- [2] Cenko, A., *Experience in the use of computational aerodynamics to predict store release characteristics*, Progress in Aerospace Sciences, 37 (2001), pp 477-495.
- [3] Cenko A, Tinoco EN, *PAN AIR - weapons, carriage and separation*. AFFDL-TR-79-3142, December 1979.
- [4] Meyer R, Cenko A, Yaros S., *An influence function method for predicting aerodynamic characteristics during weapon separation*, 12th Navy Symposium on Aeroballistics, May 1981.
- [5] Nielsen JN. et al. *A calculative method for predicting store separation trajectories at speeds up to the critical speed*, AGARD-CP-71, January 1971.
- [6] Steger JL., Dougherty FC., Benek JA., *A Chimera grid scheme*, Advances in grid generation, ASME, June 1983.
- [7] Lohner R., *Adaptive remeshing for transient problems with moving bodies*, AIAA Paper 88-3736, 1988.
- [8] Fox., J. H., *23. Generic Wing, Pylon, and Moving Finned Store*, Verification and Validation Data for Computational Unsteady Aerodynamics, RTO-TR-26, October 2000, St. Joseph Ottawa/Hill, Canada.
- [9] Newman JC, Baysal O., *Transonic Solutions of a Wing/Pylon/Finned store using hybrid domain decomposition*, AIAA Paper 92-4571, August 1992.
- [10] Parikh P, Pirzadeh S, Frink NT., *Unstructured grid solutions to a Wing/Pylon/Store configuration using VGRID3D/USM3D*, AIAA Paper 92-4572, August 1992
- [11] Meakin R., *Computations of the unsteady viscous flow about a generic Wing/Pylon/Finned-Store configuration*, AIAA Paper 92-4568, August 1992.
- [12] Madson M. et al. *TranAir computations of the flow about a Generic Wing/Pylon/Finned-store configuration*, AIAA Paper 94-0155, January 1994
- [13] Demir, H.Ö., Alemdaroğlu, N., *Uçak Kanadından Harici Yük Ayrılması*, Savunma Teknolojileri Kongresi, 24-25 Haziran 2004, Ankara.

- [14] Madson M, Talbot M., *F-16/Generic store carriage load predictions at transonic Mach numbers using TranAir*, AIAA-96-2454, June, 1996
- [15] Wey T., Martin F., *Application of the OVERFLOW code to the F-16 configuration*, AIAA-96-2459, June 1996.
- [16] Chine D. et al. *Calculation of generic store separation from an F-16 Aircraft*, AIAA-96-2455, June 1996.
- [17] Cenko, A. et al., *F/A-18C/JDAM CFD Challenge results /ACFD Challenge II* AIAA paper 2000-0795, January 2000.
- [18] Rock, S.G., and Habchi, S.D., Yeiser, C., and Oslon, M., Marwuelle, T., *A Computational Methodology for the Rapid Simulation of Jettisoned Aircraft Canopy Trajectories*, 35th Aerospace Sciences Meeting and Exhibit, January 6-10, 1997.
- [19] Hall., L., *Navier-Stokes /6-DOF Analysis of the JDAM store separation from the F/A-18C Aircraft*, AIAA Paper 99-0122, January 1999.
- [20] Chen., P.C., Liu., D.D., *Store-Separation Analyses at Subsonic and Supersonic Speeds Using a High-Order Panel Method*, AGARD 76th Fluid Dynamics Panel Meeting and Symposium on Aerodynamics of Store Integration and Separation, Ankara, Turkey, 24-28 April, 1995.
- [21] Lijewski, L. E., and Suhs, N. E., *Time-Accurate Computational Fluid Dynamics Approach to Transonic Store Separation Trajectory Prediction*, Journal of Aircraft, Vol. 31. No. 4, 1994, pp. 886-891.
- [22] Prewitt, N. C., Belk, D.M., and Maple, R. C., *Multiple Body Trajectory calculations Using the Beggar Code*, Journal of Aircraft, Vol. 36, No. 5, 1999, pp. 802-808.
- [23] Lee, S., and Park, M., Cho, K. W., and Kwon, J. H., *New Fully Automated Procedure for the Prediction of Store Trajectory*, Journal of Aircraft, Vol. 37, No. 6, 2000.
- [24] Demir, H.Ö., Alemdaroğlu, N., *Uçak Kanadından Harici Yük Ayrılması*, Kayseri V. Havacılık Sempozyumu, 13-14 Mayıs 2004, Kayseri
- [25] Demir, H.Ö., Alemdaroğlu, N., *External Store Separation from Fighter Aircraft*, AVT-108, Symposium on "Functional and Mechanical Integration of Weapons with Land and Air Vehicles," 7-10 June 2004 Williamsburg, VA, UNITED STATES
- [26] Kern, S.B., Findlay, D.B., *F/A-18C Store Carriage Loads Prediction and Mutual Interference Aerodynamics*, presented in RTO SCI Symposium on *Aircraft Weapon System Compatibility and Integration*, Chester, UK, 28-30 September 1998

- [27] Wang, Z.J., Yang, H.Q., *A Unified Conservative Zonal Interface Treatment for Arbitrarily Patched and Overlapped Grids*, 32nd Aerospace Sciences Meeting and Exhibit, January 10-13, 1994, /Reno, NV
- [28] Wang, Z.J., *A fully Conservative Structured/Unstructured Chimera Grid Scheme*, 33rd Aerospace Sciences Meeting and Exhibit, January 9-12, 1995 /Reno, NV
- [29] Wang, Z.J., Buning, P., Benek, J., *Critical Evaluation of Conservative and Non-Conservative Interface Treatment for Chimera Grids*, 33rd Aerospace Sciences Meeting and Exhibit, January 9-12, 1995 /Reno, NV
- [30] Wang, Z.J., *A Conservative Overlapped (Chimera)Grid Algorithm for Multiple Body Flows*, 34th Aerospace Sciences Meeting and Exhibit, January 15-18, 1996 /Reno, NV
- [31] CFD-FASTRAN Theory Manual, Version 2003, CFDRC Research Corporation, May 2003.
- [32] Lijewski L.E., *Transonic Euler Solutions on Mutually Interfering Finned Bodies*, AIAA Journal, Vol., 28, No. 6
- [33] Tarhan E., *Two and Three Dimensional Overset Grid Solutions of Euler/Navier-Stokes Equations*, PHD Thesis, METU, July 2003
- [34] Kurtuluş D.F., *Aerodynamic Analysis of a Full Aircraft Configuration Using a Panel Method*, M.S. Thesis, METU, January 2002
- [35] Bozkurttaş M., *Aerodynamic Analysis of External Stores on Aircraft*, M.S. Thesis, METU, November 2001
- [36] Erhan H., *Aerodynamic Analysis of Fighter Aircraft F-16 With External Stores*, M.S. Thesis, METU, January 2003